MeV-scale reheating temperature and thermalization of the neutrino background

M. Kawasaki and K. Kohri
Research Center for the Early Universe, School of Science, University of Tokyo, Tokyo 113-0033, Japan

Naoshi Sugiyama
Department of Physics, Kyoto University, Kyoto 606-8502, Japan
(Received 8 February 2000; published 20 June 2000)

The late-time entropy production by massive particle decay induces various cosmological effects in the early epoch and modifies the standard scenario. We investigate the thermalization process of the neutrinos after entropy production by solving the Boltzmann equations numerically. We find that if the large entropy is produced at $t \sim 1$ sec, the neutrinos are not thermalized very well and do not have the perfect Fermi-Dirac distribution. Then the freeze-out value of the neutron to proton ratio is altered considerably and the produced light elements, especially ^{4}He, are drastically changed. Comparing with the observational light element abundances, we find that $T_R \lesssim 0.7$ MeV is excluded at 95 % C.L. We also study the case in which the massive particle has a decay mode into hadrons. Then we find that T_R should be a little higher, i.e., $T_R \gtrsim 2.5$–4 MeV, for the hadronic branching ratio $B_h = 10^{-2} - 1$. The possible influence of late-time entropy production on the large scale structure formation and temperature anisotropies of cosmic microwave background is studied. It is expected that the future satellite experiments (MAP and PLANCK) to measure anisotropies of cosmic microwave background radiation temperature will be able to detect the vestige of the late-time entropy production as a modification of the effective number of the neutrino species $N_\nu^{\rm eff}$.

PACS number(s): 98.80.Cq, 98.70.Vc

I. INTRODUCTION

In standard big bang cosmology it has been assumed tacitly that the universe was dominated by thermal radiation at an early epoch. Even in the paradigm of modern cosmology it is commonly believed that thermal radiation was produced by the reheating process after primordial inflation and it dominated the energy of the universe at a sufficiently early epoch. Here we ask the following: ''How early should the universe be dominated by radiation in order for standard big bang cosmology to succeed?'' We could say that the energy of the universe should be dominated by the radiation at least before the beginning of the big bang nucleosynthesis (BBN) epoch. In this paper we answer the above question.

The various models of modern particle physics beyond the standard model predict a number of unstable massive particles which have long lifetimes and decay at about the BBN epoch. The energy density of the nonrelativistic particles or the oscillation energy density of the scalar fields (inflaton and so on) decreases as $\rho_{\rm NR}(t) \propto a(t)^{-3}$, where $a(t)$ is a scale factor. On the other hand, since the radiation energy density decreases more rapidly $\rho(t) \propto a(t)^{-4}$, if the energy density of the massive nonrelativistic particles or the oscillating scalar fields is large enough, it immediately dominates the universe as it expands, and the universe necessarily becomes matter dominated until the cosmic time reaches their lifetime. When the particles decay into standard particles (e.g., photon and electron), they produce the large entropy and the universe becomes radiation dominated again. It is expected that such a process would change the initial condition for the standard big bang scenario. We call the process ''late-time entropy production.''

Now we have some interesting candidates for late-time entropy production in models based on supersymmetry (SUSY). It is known that gravitino and Polonyi fields which exist in local SUSY (i.e., supergravity) theories have masses of $\sim \mathcal{O}(100\ \text{GeV}-10\ \text{TeV})$ [1]. In addition they have long lifetimes because they interact with the other particle only through gravity. For example, since the Polonyi field [2] which has a heavy mass of ~ 10 TeV cannot be diluted by usual inflation, it immediately dominates the universe and decays at the BBN epoch. Moreover it is also known that in superstring theories there exist many light fields called dilatons and moduli which have similar properties to the Polonyi field.

Recently Lyth and Stewart [3] considered mini-inflation called ''thermal inflation'' which dilutes the above dangerous scalar fields. In the thermal inflation scenario, however, the flaton field which is responsible for the thermal inflation decays at late times. In particular, if the Polonyi (moduli) mass is less than ~ 1 GeV which is predicted in the framework of gauge-mediated SUSY breaking models [4], the sufficient dilution requires that the flaton decays just before BBN [5]. Thus, in thermal inflation models, one should take care of the late-time entropy production.

To keep the success of BBN, any long-lived massive particle or the coherent oscillation of any scalar field which dominates the universe at that time must finally decay into the standard particles before the beginning of BBN. Moreover the decay products would have to be quickly thermalized through scattering, annihilation, pair creation, and further decays and make the thermal bath of photons, electrons, and neutrinos. Concerning photons and electrons which electromagnetically interact, the interaction rate is much more rapid than the Hubble expansion rate at that time. Therefore it is expected that the photons and electrons which are produced in the decay and subsequent thermalization processes are efficiently thermalized.

TABLE I. Matrix elements for electron neutrino interactions. G_F is the Fermi coupling constant. Here we take $C_V=\frac{1}{2}+2\sin^2\theta_W$, $C_A=\frac{1}{2}$ and the weak mixing angle $\sin^2\theta_W\simeq 0.231$.

Process			$S\|M\|^2$
ν_e+e^-	$\rightarrow$	ν_e+e^-	$32G_F^2[(C_V+C_A)^2(p_1p_2)^2+(C_V-C_A)^2(p_1p_4)^2]$
ν_e+e^+	$\rightarrow$	ν_e+e^+	$32G_F^2[(C_V-C_A)^2(p_1p_2)^2+(C_V+C_A)^2(p_1p_4)^2]$
$\nu_e+\overline{\nu_e}$	$\rightarrow$	e^++e^-	$32G_F^2[(C_V+C_A)^2(p_1p_4)^2+(C_V-C_A)^2(p_1p_3)^2]$

The problem is that neutrinos can interact only through the weak interaction. Since massive scalar particles such as the modulus and the Polonyi field have small branching ratios into neutrinos due to the chirality flip and small neutrino masses, it is expected that neutrinos are produced only through annihilation of electrons and positrons. In the standard big bang cosmology the neutrinos usually decouple from the electromagnetic thermal bath at about $T\simeq 2-3$ MeV. Therefore it is approximately inferred that they cannot be sufficiently thermalized at temperatures $T\lesssim$ a few MeV. Namely, the reheating temperature after the entropy production process should be high enough to thermalize the neutrinos. Although people had always used rough constraints on reheating temperatures between 1–10 MeV, in the previous paper [6] we pointed out that neutrino thermalization is the most crucial for successful BBN. In this paper we describe the method to obtain the neutrino spectrum and the formulations to integrate a set of Boltzmann equations numerically , and we study the constraint on the reheating temperature using the obtained neutrino spectrum and the full BBN network calculations with revised observational light element abundances.

The above constraint is almost model independent and hence conservative because we only assume that the massive particle decay produces the entropy. However, a more stringent constraint can be obtained if we assume a decay mode into quarks or gluons. In this case some modifications are needed for the above description. When high-energy quark-antiquark pairs or gluons are emitted, they immediately fragment into a lot of hadrons (pions, kaons, protons, neutrons, etc.). It is expected that they significantly influence the freeze-out value of the neutron to proton ratio at the beginning of BBN through the strong interaction with the ambient protons and neutrons. In a previous paper [6] we did not consider such hadron injection effects on BBN. Therefore we carefully treat the hadron injection effects in the present paper.

For another constraint, the late-time entropy production may induce significant effects on the anisotropies of the cosmic microwave background radiation (CMB). Lopez *et al.* [7] pointed out that the CMB anisotropies are very sensitive to the equal time of matter and radiation. When the reheating temperature is so low that neutrinos are not sufficiently thermalized, the radiation density which consists of photons and neutrinos becomes less than that in the standard big bang scenario. There may be distinguishable signals in the CMB anisotropies, such as a modification of the effective number of neutrino species $N_\nu^{\rm eff}$. With the present angular resolutions and sensitivities of Cosmic Background Explorer (COBE) observation [8] it is impossible to set a constraint on $N_\nu^{\rm eff}$ but it is expected that future satellite experiments such as the Microwave Anisotropy Probe (MAP) [9] and Planck [10] will gives us a useful information about $N_\nu^{\rm eff}$. In addition the above effect may also induce signals in the observed power spectrum of the density fluctuation for the large scale structure as a modification of the epoch of the matter-radiation equality.

The paper is organized as follows. In Sec. II we introduce the formulation of the basic equations and the physical parameters. In Sec. III we briefly review the current status of the observational light element abundances. In Sec. IV we study the spectra of the electron neutrino and the mu(tau) neutrino by numerically solving the Boltzmann equations, and the constraints from the BBN are obtained there. In Sec. V we investigate the additional effects in the hadron injection by the massive particle decay. In Sec. VI we consider the other constraints which come from observations for large scale structures and anisotropies of CMB. Section VII is devoted to conclusions. In the Appendix we introduce the method of the reduction for the nine-dimensional integrals into one dimension.

II. FORMULATION OF NEUTRINO THERMALIZATION

A. Reheating temperature

In order to discuss the late-time entropy production process, we should formulate the equations which describe the physical process. Here the reheating temperature T_R is an appropriate parameter to characterize late-time entropy production. We define the reheating temperature T_R by

$$\Gamma\equiv 3H(T_R), \tag{1}$$

where Γ is the decay rate ($=\tau^{-1}$) and $H(T_R)$ is the Hubble parameter at the decay epoch ($t=\tau$).[1] The Hubble parameter is expressed by

$$H=\left(\frac{g_*\pi^2}{90}\right)^{1/2}\frac{T_R^2}{M_G}, \tag{2}$$

[1]Since the actual decay is not instantaneous, the matter-dominated universe smoothly changes into radiation-dominated one. Thus it is rather difficult to clearly identify the reheating temperature by observing the evolution of the cosmic temperature. Instead we ''define'' the reheating temperature formally by Eq. (1).

TABLE II. Matrix elements for muon neutrino or tau neutrino interactions. G_F is the Fermi coupling constant. Here we take $\tilde{C}_V = C_V - 1 = -\frac{1}{2} + 2\sin^2\theta_W$, $\tilde{C}_A = C_A - 1 = -\frac{1}{2}$ and the weak mixing angle $\sin^2\theta_W \simeq 0.231$.

Process			$S\|M\|^2$
$\nu_\mu + e^- \to \nu_\mu + e^-$			$32G_F^2[(\tilde{C}_V+\tilde{C}_A)^2(p_1p_2)^2+(\tilde{C}_V-\tilde{C}_A)^2(p_1p_4)^2]$
$\nu_\mu + e^+ \to \nu_\mu + e^+$			$32G_F^2[(\tilde{C}_V-\tilde{C}_A)^2(p_1p_2)^2+(\tilde{C}_V+\tilde{C}_A)^2(p_1p_4)^2]$
$\nu_\mu + \overline{\nu_\mu} \to e^+ + e^-$			$32G_F^2[(\tilde{C}_V+\tilde{C}_A)^2(p_1p_4)^2+(\tilde{C}_V-\tilde{C}_A)^2(p_1p_3)^2]$

where g_* is the statistical degrees of freedom for the massless particles and M_G is the reduced Plank mass ($=2.4 \times 10^{18}$ GeV). Then the reheating temperature is given by

$$T_R = 0.554\sqrt{\Gamma M_G}. \tag{3}$$

Here we have used $g_* = 43/4$. From Eq. (3), we can see that the reheating temperature has a one to one correspondence with the lifetime of the parent massive particle.

Here we define the effective number of neutrino species $N_\nu^{\rm eff}$ as a parameter which characterize the time evolution of the energy density of neutrinos. Here $N_\nu^{\rm eff}$ is defined by

$$N_\nu^{\rm eff} \equiv \frac{\rho_{\nu_e} + \rho_{\nu_\mu} + \rho_{\nu_\tau}}{\rho_{\rm std}}, \tag{4}$$

where $\rho_{\rm std}$ is the total neutrino energy density in the standard big bang model (i.e., no late-time entropy production and three neutrino species).

B. Basic equations

When the massive particle ϕ which is responsible for the late-time entropy production decays, all emitted particles except neutrinos are quickly thermalized and make a thermal bath with temperature $\sim T_R$. For the relatively low reheating temperature $T_R \lesssim 10$ MeV neutrinos are slowly thermalized. If the entropy production caused by the massive scalar particles such as moduli, Polonyi and flaton fields, the decay branching ratio into neutrinos is very small because the decay is suppressed by the chirality flip and vanishes for small neutrino masses. Therefore we ignore the branching into neutrinos. Generally speaking, however, a fermion such as gravitino might be a candidate, instead of scalar particles. In this case, it may have a net branching ratio into neutrinos. However, in this paper, we assume that the branching ratio into neutrinos is negligible and neutrinos are produced only through annihilation of electrons and positrons, i.e., $e^+ + e^- \to \nu_i + \overline{\nu_i} (i = e, \mu, \tau)$ in order to avoid discussing specific models. The evolution of the distribution function f_i of the neutrino ν_i is described by the momentum-dependent Boltzmann equation [11]

$$\frac{\partial f_i(\boldsymbol{p},t)}{\partial t} - H(t)\boldsymbol{p}\frac{\partial f_i(p,t)}{\partial \boldsymbol{p}} = C_{i,\rm coll}, \tag{5}$$

where the right-hand side is the total collision term.[2] When the reaction is two-body scattering $1+2 \to 3+4$, it is given by the expression

$$C_{i,\rm coll} = \frac{1}{2E_1}\sum \int \frac{d^3p_2}{2E_2(2\pi)^3}\frac{d^3p_3}{2E_3(2\pi)^3}\frac{d^3p_4}{2E_4(2\pi)^3} \times (2\pi)^4\delta^{(4)}(p_1+p_2-p_3-p_4) \times \Lambda(f_1,f_2,f_3,f_4)S|M|^2_{12\to 34}, \tag{6}$$

where $|M|^2$ is the scattering amplitude summed over spins of all particles, S is the symmetrization factor which is 1/2 for identical particles in initial and final states, $\Lambda = f_3f_4(1-f_1)(1-f_2) - f_1f_2(1-f_3)(1-f_4)$ is the phase space factor including Pauli blocking of the final states. Then the total collision term $C_{i,\rm coll}$ is expressed by

$$C_{i,\rm coll} = C_{i,\rm ann} + C_{i,\rm scat}, \tag{7}$$

where $C_{i,\rm ann}$ is the collision term for annihilation processes and $C_{i,\rm scat}$ is the collision term for elastic scattering processes. Here we consider the following processes:

$$\nu_i + \nu_i \leftrightarrow e^+ + e^-,$$

$$\nu_i + e^\pm \leftrightarrow \nu_i + e^\pm.$$

In this paper we have treated neutrinos as Majorana ones (i.e., $\nu = \overline{\nu}$). It should be noted that there are no differences between Majorana neutrinos and Dirac ones as long as they are massless, and since the temperature is $\mathcal{O}$(MeV) at least in this situation, we could have treated them as if they were

[2]The integrated Boltzmann equation [12] is not adequate in the present problem. As we show in Sec. IV, the spectral shape of the momentum distribution obtained by our scheme is much different from the equilibrium one. It should be noticed that the integrated Boltzmann equation assumes that the shape of the momentum distribution is the same as the equilibrium one. Thus we should solve the momentum dependent Boltzmann equation.

massless particles. The relevant reactions are presented in Table I for ν_e and Table II for ν_μ and ν_τ.[3]

The collision terms are quite complicated and expressed by nine-dimensional integrations over momentum space. However, if we neglect electron mass and assume that electrons obey the Boltzmann distribution $e^{-p/T}$, the collision terms are simplified to one-dimensional integration form.[4] Then $C_{i,\mathrm{ann}}$ is given by [15,16]

$$C_{i,\mathrm{ann}} = -\frac{1}{2\pi^2}\int p_i'^2 dp_i' (\sigma v)_i [f_i(p_i) f_i(p_i') - f_{eq}(p_i) f_{eq}(p_i')], \tag{8}$$

where $f_{eq}[=1/(e^{p_i/T}+1)]$ is the equilibrium distribution and $(\sigma v)_i$ is the differential cross sections given by

$$(\sigma v)_e = \frac{4G_F^2}{9\pi}(C_V^2 + C_A^2) p p', \tag{9}$$

$$(\sigma v)_{\mu,\tau} = \frac{4G_F^2}{9\pi}(\tilde{C}_V^2 + \tilde{C}_A^2) p p', \tag{10}$$

where we take

$$C_V = \tfrac{1}{2} + 2\sin^2\theta_W, \quad C_A = \tfrac{1}{2}, \qquad \tilde{C}_V = C_V - 1 \quad (\tilde{C}_A = C_A - 1), \tag{11}$$

and θ_W is Weinberg angle ($\sin^2\theta_W \simeq 0.231$) [27].

As for elastic scattering processes, $C_{i,\mathrm{scat}}$ is also simplified to one dimensional integration (see the Appendix), and it is expressed as

$$C_{i,\mathrm{scat}} = \frac{G_F^2}{2\pi^3}(C_V^2 + C_A^2)\Bigg[-\frac{f_i}{p_i^2}\Bigg(\int_0^{p_i} dp_i' F_1(p_i, p_i') \times [1 - f_i(p_i')] + \int_{p_i}^{\infty} dp_i' F_2(p_i, p_i')[1 - f_i(p_i')] \Bigg) + \frac{1 - f_i(p_i)}{p_i^2}\Bigg(\int_0^{p_i} dp_i' B_1(p_i, p_i') f_i(p_i') + \int_{p_i}^{\infty} dp_i' B_2(p_i, p_i') f_i(p_i') \Bigg) \Bigg], \tag{12}$$

where $(C_V^2 + C_A^2)$ should be replaced by $(\tilde{C}_V^2 + \tilde{C}_A^2)$ for $i = \mu, \tau$, and the functions F_1, F_2, B_1, B_2 are given by

$$F_1(p,p') = D(p,p') + E(p,p') e^{-p'/T},$$

$$F_2(p,p') = D(p',p) e^{(p-p')/T} + E(p,p') e^{-p'/T},$$

$$B_1(p,p') = F_2(p',p), \quad B_2(p,p') = F_1(p',p), \tag{13}$$

where

$$D(p,p') = 2T^4(p^2 + p'^2 + 2T(p - p') + 4T^2),$$

$$E(p,p') = -T^2[p^2 p'^2 + 2pp'(p + p')T + 2(p + p')^2 T^2 + 4(p + p')T^3 + 8T^4]. \tag{14}$$

Together with the above Boltzmann equations, we should solve the energy-momentum conservation equation in the expanding universe:

$$\frac{d\rho(t)}{dt} = -3H(t)[\rho(t) + P(t)], \tag{15}$$

where $\rho(t) = \rho_\phi + \rho_\gamma + \rho_e + \rho_\nu$ is the total energy density of ϕ's, photons, electrons, and neutrinos and is given by

$$\rho(t) = \rho_\phi(t) + \frac{\pi^2 T_\gamma^4}{15} + \frac{2}{\pi^2}\int \frac{dq q^2 E_e}{\exp(E_e/T_\gamma) + 1} + \frac{1}{\pi^2}\int dq q^3 f_{\nu_e}(q) + \frac{2}{\pi^2}\int dq q^3 f_{\nu_\mu}(q), \tag{16}$$

where $E_e = \sqrt{q^2 + m_e^2}$ is the electron energy. $P(t) \equiv P_\gamma(t) + P_{e^\pm}(t) + P_\nu(t)$ is the total pressure,

$$P(t) = \frac{\pi^2 T_\gamma^4}{45} + \frac{2}{\pi^2}\int \frac{dq q^4}{3E_e[\exp(E_e/T_\gamma) + 1]} + \frac{1}{3\pi^2}\int dq q^3 f_{\nu_e}(q) + \frac{2}{3\pi^2}\int dq q^3 f_{\nu_\mu}(q). \tag{17}$$

$H(t)$ is the Hubble parameter,

[3]Here we neglect the neutrino self-interactions. This may lead to underestimate the kinetic equilibrium rate for high reheating temperatures. However, we think that this effect does not change the results very much. The interactions between electrons and neutrinos are the most important because they transfer the energy of the thermal bath to neutrinos. The self-interactions of the neutrinos cannot increase the energy density of neutrinos but mainly change their momentum distribution. Furthermore, the neutrino number densities are much smaller than the electron number density at low reheating temperature with which we are concerned. Thus differences caused by the neutrino self interactions are expected to be small.

[4]The errors due to neglecting the electron mass are small and the deviation is just a few percent. We list the reasons as follows. The difference between Fermi-Dirac and Maxwell-Boltzmann distribution "df" is less than 1 at most $df < 1.0$. The week interaction rate is almost expressed by $\langle \sigma v \rangle n_e / H(t)$, where $\langle \sigma v \rangle \sim G_F^2 m_e^2$ and n_e is an electron number density. Then the error is at most estimated by $\langle \sigma_W v \rangle n_e / H(t) \times df \lesssim 10^{-2}$ (for $T \lesssim 0.5$ MeV). Therefore the deviation is a few percent and neglecting the electron mass does not change the results. The other methods of the approximation to reduce the integral from nine to two dimensions in which the electron mass is not neglected are presented in Refs. [13,14].

$$H(t)=\frac{\dot{a}(t)}{a(t)}=\frac{1}{\sqrt{3}M_G}\sqrt{\rho(t)}. \tag{18}$$

The time evolution equation of ρ_ϕ is given by

$$\frac{d\rho_\phi}{dt}=-\Gamma\rho_\phi-3H\rho_\phi. \tag{19}$$

We solve the time evolution of the photon temperature instead of Eq. (15),

$$\frac{dT_\gamma}{dt}=-\frac{-\rho_\phi/\tau_\phi+4H\rho_\gamma+3H(\rho_{e^\pm}+P_{e^\pm})+4H\rho_\nu+d\rho_\nu/dt}{\partial\rho_\gamma/\partial T_\gamma|_{a(t)}+\partial\rho_{e^\pm}/\partial T_\gamma|_{a(t)}}, \tag{20}$$

together with Eqs. (5), (18), and (19).

III. OBSERVATIONAL LIGHT ELEMENT ABUNDANCES

In this section we briefly show the current status of the observational light element abundances. Concerning the deuterium abundance, the primordial D/H is measured in the high redshift quasistellar orbject (QSO) absorption systems. For the most reliable D abundance, we adopt the following value which is obtained by the clouds at $z=3.572$ towards $Q1937-1009$ and at $z=2.504$ towards $Q1009+2956$ [17],

$$\mathrm{D/H}=(3.39\pm0.25)\times10^{-5}. \tag{21}$$

On the other hand, recently the high deuterium abundance is reported in relatively low redshift absorption systems at $z=0.701$ towards $Q1718+4807$ [18], $\mathrm{D/H}=(2.0\pm0.5)\times10^{-4}$. Another group also observes the clouds independently [19]. However, because they do not have full spectra of the Lyman series, the analyses would be unreliable. More recently Kirkman *et al.* [20] observed the quasar absorption systems at $z=2.8$ towards $Q0130-4021$ and they obtain the upper bound $\mathrm{D/H}\lesssim6.7\times10^{-5}$. Moreover Molaro *et al.* reported $\mathrm{D/H}\simeq1.5\times10^{-5}$ which was observed in the absorber at $z=3.514$ towards APM 08279+5255 although it has the large systematic errors in the hydrogen column density [21]. Considering the current situation, we do not adopt the high deuterium value in this paper.

The primordial ^{4}He mass fraction Y_p is observed in the low metalicity extragalactic HII regions. Since ^{4}He is produced with oxygen in the star, the primordial value is obtained to regress to the zero metalicity $\mathrm{O/H}\to0$ for the observational data. Using the 62 blue compact galaxies (BCG) observations, it was reported that the primordial Y is rela-

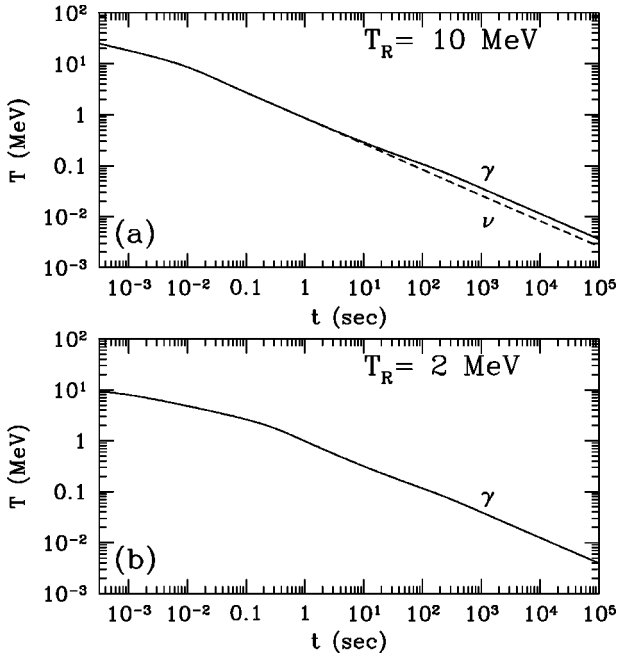

FIG. 1. Time evolution of the cosmic temperature (a) for $T_R=10$ MeV, and (b) for $T_R=2$ MeV. The dashed line denotes the neutrino temperature which can be defined only when they are thermalized sufficiently and have the perfect Fermi-Dirac distribution.

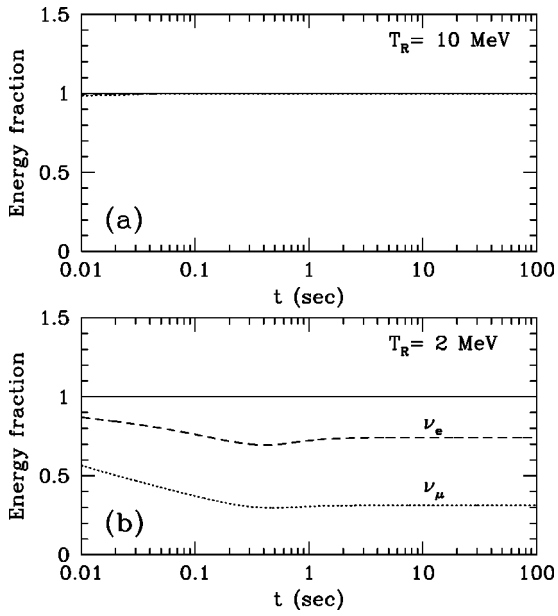

FIG. 2. Time evolution of the fraction of the energy density of ν_e (solid curve) and ν_μ (dashed curve) to that of the standard big bang scenario for (a) $T_R=10$ MeV and (b)$T_R=2$ MeV. Since the interaction of ν_τ is as same as ν_μ, the curve of ν_μ also represents ν_τ.

tively ‘‘ low,’’ $Y_p \simeq 0.234$ [22]. However, recently it is claimed that HeI stellar absorption is an important effect though it was not included in the previous analysis [23] properly. They found the relatively ‘‘high’’ primordial value $Y_p = 0.245 \pm 0.004$. More recently Fields and Olive [24] also reanalyze the data including the HeI absorption effect and they obtain

$$Y_p = 0.238 \pm (0.002)_{\rm stat} \pm (0.005)_{\rm syst}, \tag{22}$$

where the first error is the statistical uncertainty and the second error is the systematic one. We adopt the above value as the observational Y_p.

The primordial ^{7}Li/H is observed in the Pop II old halo stars. In general a halo star whose surface effective temperature is low (the mass is small), has the deep convective zone. For such a low-temperature star, the primordial ^{7}Li is considerably depleted in the warm interior of the star. On the other hand for the high-temperature stars ($T_{\rm eff} \gtrsim 5500$ K), it is known that the primordial abundance is not changed and they have a ‘‘plateau’’of the ^{7}Li as a function of the effective temperature. In addition, though it is also known that ^{7}Li/H decreases with decreasing Fe/H, ^{7}Li still levels off at lower metalicity, $[{\rm Fe/H}] \lesssim -1.5$, in the plateau stars. We adopt the recent measurements which are observed by Bonifacio and Molaro [25]. They observed 41 old halo stars which have the plateau. We take the additional larger systematic error, because there may be underestimates in the stellar depletion and the production by the cosmic ray spallation. Then we obtain

$$\log_{10}(^7{\rm Li}/H) = -9.76 \pm (0.012)_{\rm stat} \pm (0.05)_{\rm syst} \pm (0.3)_{\rm add}. \tag{23}$$

IV. NEUTRINO THERMALIZATION AND BBN

A. Time evolution of neutrino spectrum

The evolution of the cosmic temperature T is shown in Fig. 1(a) for $T_R = 10$ MeV and (b) for $T_R = 2$ MeV. In Fig. 1(a), it is seen that the temperature decreases slowly as $t^{-1/4}$, i.e., $a^{-3/8}$ before the decay epoch, $t \simeq \Gamma^{-1} (\simeq 5 \times 10^{-2}$ sec) which corresponds to $T_R = 10$ MeV. This is because the actual decay is not instantaneous and ϕ decays into radiation continuously at the rate Γ [26]. Then the universe is still in matter dominated (MD). After the decay epoch $t \gg \Gamma^{-1}$, all ϕ particles decay and the temperature decreases as a^{-1} and $t^{-1/2}$. Then the universe becomes radiation-dominated epoch. Since at the temperature $T \lesssim 0.5$ MeV ($t \gtrsim 3$ sec), electrons and positrons annihilate into photons $e^+ e^- \to 2\gamma$, the temperature is slightly heated. From Fig. 1(b) we can see that the temperature decreases as $t^{-1/4}$ until the decay epoch ($t \lesssim 0.1$ sec) which corresponds to $T_R = 2$ MeV. After the decay epoch, the temperature decreases as $t^{-1/2}$ [radiation dominated (RD)]. In the actual computation we take an initial condition that there exists the net radiation energy density though the universe is in MD. This represents the situation that the massive particle necessarily dominated the universe as it expands. On the other hand, even if there are at first no radiation $\rho_R \simeq 0$, i.e., $T \simeq 0$ which corresponds to the initial condition of the oscillation epoch after the primordial inflation or thermal inflation, the cosmic temperature immediately tracks the same curve $t^{-1/4}$ and then their decay establish the radiation dominated universe $T \propto t^{-1/2}$. Therefore our treatment is quite a general picture for each entropy production scenario and it does not depend on whether the net initial radiation energy exists or not, only if once the unstable nonrelativistic particles dominate the energy density of the universe.

In Fig. 2 we show the evolutions of ρ_{ν_e} and ρ_{ν_μ} ($=\rho_{\nu_\tau}$) (a) for $T_R = 10$ MeV and (b) 2 MeV. From Fig. 2(a) we can see that if $T_R = 10$ MeV, cosmic energy density is as same as the case of standard big bang cosmology. As shown in Fig. 2(b), however, the energy density of each neutrino species for $T_R = 2$ MeV is smaller than the case of standard scenario. Since the electron neutrinos interact with electrons and positrons through both charged and neutral currents, they are more effectively produced from the thermal bath than the other neutrinos which have only neutral current interactions. The final distribution functions f_e and $f_\mu (= f_\tau)$ are shown in Fig. 3 (a) for $T_R = 10$ MeV and (b) 2 MeV. For $T_R = 10$ MeV, each neutrino is thermalized well and the perfect Fermi-Dirac distribution is established. For $T_R = 2$ MeV, however, the distributions are not thermal equilibrium forms.[5]

In Fig. 4 we can see the change of the effective number of neutrino species $N_\nu^{\rm eff}$ as a function of the reheating temperature T_R. If $T_R \gtrsim 7$ MeV, $N_\nu^{\rm eff}$ is almost equal to 3 and

[5]As we noted in Sec. II, we must not use the integrated Boltzmann equation instead of the momentum-dependent Boltzmann equation in the present problem because the former assumes the equilibrium distribution. To see this, let us define the ratio R_E for a neutrino species by $R_E = (\rho_\nu / n_\nu)/(3.151 \tilde{T}_\nu)$, where ρ_ν is the neutrino energy density, n_ν is the neutrino number density, $\tilde{T}_\nu$ is the effective neutrino temperature which is defined by the neutrino number density as $\tilde{T}_\nu \equiv \{2\pi^2/[3\zeta(3)] n_\nu\}^{1/3}$. Here both ρ_ν and n_ν are computed by integrating the neutrino distribution function which is obtained by solving the momentum-dependent Boltzmann equation. R_E approximately represents the ratio of the mean energy per neutrino to the thermal equilibrium one. If the neutrino is in thermal equilibrium, R_E is unity. In the case of the integrated Boltzmann equation, because it is assumed that the shape of the neutrino distribution is the same as the equilibrium one at any time, R_E is necessarily unity. On the other hand, in the case of our scheme, i.e., the momentum dependent Boltzmann equation, R_E cannot be unity. We have computed the ratio R_E in some representative reheating temperatures for electron neutrinos and have found that they deviated from unity more at the lower reheating temperatures, $R_E = 1.00$, 1.03, and 1.50 (for $T_R = 10$, 3, and 1 MeV). Moreover at reheating temperatures lower than 1 MeV, the deviation is much larger. This result tells us that the neutrino distribution deviates from the thermal equilibrium shape considerably at low reheating temperatures and we should solve the momentum-dependent Boltzmann equation. R_E has the tendency to increase as the reheating temperature decreases. This is because neutrinos are produced by the annihilation of electron-positron pairs whose mean energy per particle is larger than that of neutrinos.

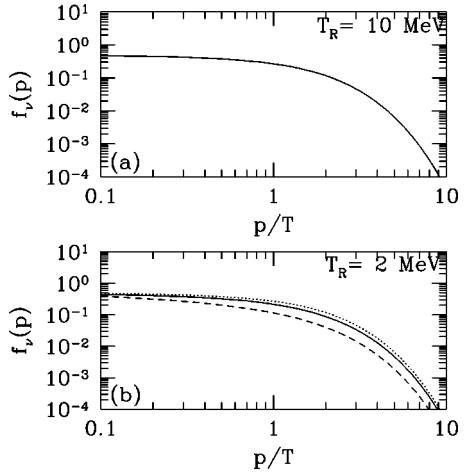

FIG. 3. Distribution function of ν_e (solid curve) and ν_μ (dashed curve) (a)for $T_R=10$ MeV and (b)for $T_R=2$ MeV. The dotted curve is the Fermi-Dirac distribution function. Since the interaction of ν_τ is as same as ν_μ, the curve of ν_μ also represents ν_τ.

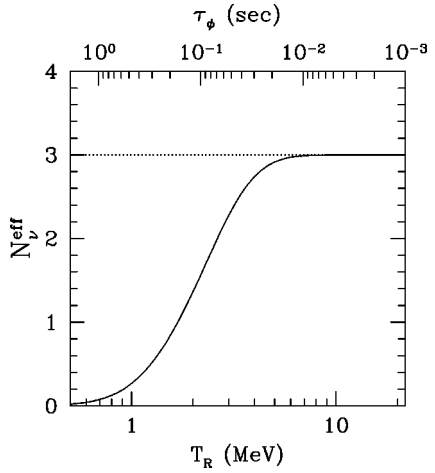

FIG. 4. Effective number of neutrino species $N_\nu^{\rm eff}$ as a function of reheating temperature T_R. The top horizontal axis denotes the lifetime which corresponds to T_R.

neutrinos are thermalized very well. We can assume that it corresponds to the initial condition which has always been used for standard big bang cosmology. On the other hand, if $T_R \lesssim 7$ MeV, $N_\nu^{\rm eff}$ becomes smaller than 3.

B. Neutrino thermalization and neutron to proton ratio

If the neutrinos are not thermalized sufficiently and do not have the perfect Fermi-Dirac distribution, i.e., in this case there is the deficit of the neutrino distribution due to the low reheating temperature, it considerably influences the produced light element abundances. In particular, the abundance of the primordial ^{4}He is drastically changed. The change of the neutrino distribution function influences the neutrino energy density and the weak interaction rates between protons and neutrons. At the beginning of BBN ($T\sim 1$–0.1 MeV) the competition between the Hubble expansion rate H and the weak interaction rates $\Gamma_{n\leftrightarrow p}$ determines the freeze-out value of neutron to proton ratio n/p. After the freeze-out time, neutrons can change into protons only through the free decay with the lifetime τ_n. Since ^{4}He is the most stable light element and the almost all neutrons are synthesized into ^{4}He, the abundance of the primordial ^{4}He is sensitive to the freeze-out value of neutron to proton ratio.

If the neutrino energy density gets smaller than that of the standard BBN (SBBN), Hubble expansion rate which is proportional to the square of the total energy density is also decreased. Then the freeze out time becomes later and the β equilibrium between neutrons and protons continues for longer time. As a result less neutrons are left. In this case the predicted ^{4}He is less than the prediction of SBBN. The effect due to the speed-down expansion is approximately estimated by

$$\Delta Y \simeq -0.1(-\Delta\rho_{\rm tot}/\rho_{\rm tot}), \tag{24}$$

where Y is the mass fraction of ^{4}He and $\rho_{\rm tot}$ is the total energy density of the universe.

Moreover, when the electron neutrino is not thermalized, there is an interesting effect by which more ^{4}He are produced. The weak reaction rates are computed by integrating neutrino distribution functions which are obtained by solving Boltzmann equations numerically. Using the neutrino distribution functions, the six weak interaction rates between neutrons and protons are represented by

$$\Gamma_{n\to pe^-\bar{\nu}_e} = K\int_0^{Q-m_e} dp_{\nu_e}\Bigg[\sqrt{(p_{\nu_e}-Q)^2-m_e^2}\times(Q-p_{\nu_e})\frac{p_{\nu_e}^2}{1+e^{(p_{\nu_e}-Q)/T_\gamma}}[1-f_{\nu_e}(p_{\nu_e})]\Bigg], \tag{25}$$

$$\Gamma_{ne^+\to p\bar{\nu}_e} = K\int_{Q+m_e}^{\infty} dp_{\nu_e}\Bigg[\sqrt{(p_{\nu_e}-Q)^2-m_e^2}\times(p_{\nu_e}-Q)\frac{p_{\nu_e}^2}{e^{(p_{\nu_e}-Q)/T_\gamma}+1}[1-f_{\nu_e}(p_{\nu_e})]\Bigg], \tag{26}$$

$$\Gamma_{n\nu_e\to pe^-} = K\int_0^{\infty} dp_{\nu_e}\Bigg[\sqrt{(p_{\nu_e}+Q)^2-m_e^2}\times(p_{\nu_e}+Q)\frac{p_{\nu_e}^2}{1+e^{-(p_{\nu_e}+Q)/T_\gamma}}f_{\nu_e}(p_{\nu_e})\Bigg], \tag{27}$$

$$\Gamma_{pe^-\bar{\nu}_e\to n}=K\int_0^{Q-m_e}dp_{\nu_e}\Bigg[\sqrt{(p_{\nu_e}-Q)^2-m_e^2}\times(Q-p_{\nu_e})\frac{p_{\nu_e}^2}{e^{-(p_{\nu_e}-Q)/T_\gamma}+1}f_{\nu_e}(p_{\nu_e})\Bigg], \tag{28}$$

$$\Gamma_{pe^-\to n\nu_e}=K\int_0^{\infty}dp_{\nu_e}\Bigg[\sqrt{(p_{\nu_e}+Q)^2-m_e^2}\times(Q+p_{\nu_e})\frac{p_{\nu_e}^2}{e^{(p_{\nu_e}+Q)/T_\gamma}+1}[1-f_{\nu_e}(p_{\nu_e})]\Bigg], \tag{29}$$

$$\Gamma_{p\bar{\nu}_e\to ne^+}=K\int_{Q+m_e}^{\infty}dp_{\nu_e}\Bigg[\sqrt{(p_{\nu_e}-Q)^2-m_e^2}\times(Q-p_{\nu_e})\frac{p_{\nu_e}^2}{1+e^{-(p_{\nu_e}-Q)/T_\gamma}}f_{\nu_e}(p_{\nu_e})\Bigg], \tag{30}$$

where $Q=m_n-m_p=1.29$ MeV and K is a normalization factor which is determined by the neutron life time τ_n as $K\simeq(1.636\tau_n)^{-1}$ and τ_n is obtained by the experiments [27]. From the above equations we can see that if neutrino and antineutrino distribution functions are decreased, both β decay rates $\Gamma_{n\to p}=\Gamma_{n\to pe^-\bar{\nu}_e}+\Gamma_{ne^+\to p\bar{\nu}_e}+\Gamma_{n\nu_e\to pe^-}$ and $\Gamma_{p\to n}=\Gamma_{pe^-\bar{\nu}_e\to n}+\Gamma_{pe^-\to n\nu_e}+\Gamma_{p\bar{\nu}_e\to ne^+}$ are simultaneously decreased by the following reasons. The dominant effects by the deficit of the distribution functions are to decrease the rates $\Gamma_{n\nu_e\to pe^-}$, $\Gamma_{pe^-\bar{\nu}_e\to n}$ and $\Gamma_{p\bar{\nu}_e\to ne^+}$ which have the neutrino or anti-neutrino in the initial state. On the other hand, though the other rates $\Gamma_{n\to pe^-\bar{\nu}_e}$, $\Gamma_{ne^+\to p\bar{\nu}_e}$, and $\Gamma_{pe^-\to n\nu_e}$ which have the neutrino or anti-neutrino in the final state are slightly increased due to Fermi-blocking factor $(1-f_\nu)$, the ratio of the difference Δf_ν to $(1-f_\nu)$ is much smaller than that of Δf_ν to f_ν, i.e.,

$$|\Delta f_\nu/(1-f_\nu)|\ll|\Delta f_\nu/f_\nu| \quad \text{for} \quad f_\nu\ll 1. \tag{31}$$

Therefore, the enhancement is small and the latter effect is not important. In total, both weak interaction rates $\Gamma_{n\to p}$ and $\Gamma_{p\to n}$ decrease and become smaller than those of SBBN. In Fig. 5 the weak interaction rates $\Gamma_{n\to p}$ and $\Gamma_{p\to n}$ are plotted. The solid lines denote the case of $T_R=10$ MeV which corresponds to the standard big bang scenario. The dotted lines denote the case of $T_R=1$ MeV. In the plot we can see that the insufficient thermalization of the neutrino distributions derives the changes of the weak interaction rates.

The decrease of weak interaction rates gives significant effects on the abundance of ^{4}He. When the weak interaction rate $\Gamma_{n\leftrightarrow p}$ decreases, the Hubble expansion rate becomes more rapid than that of the weak interaction rate earlier.

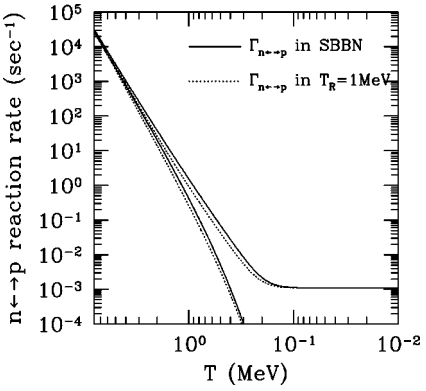

FIG. 5. Weak interaction rates ($\sec^{-1}$) between neutron and proton. The upper curves are $\Gamma_{n\to p}$. The lower curves are $\Gamma_{p\to n}$. The solid lines denote the case of $T_R=10$ MeV which corresponds to the standard big bang scenario. The dotted lines denote the case of $T_R=1$ MeV in the late-time entropy production scenario. Notice that $\Gamma_{n\to p}^{-1}$ reaches $\tau_n=887$ sec at low temperature.

Namely, the freeze-out time becomes earlier. Then the freeze-out value of neutron to proton ratio becomes larger than in SBBN and it is expected that the predicted ^{4}He abundance becomes larger. The above effect is approximately estimated by

$$\Delta Y\simeq+0.19(-\Delta\Gamma_{n\leftrightarrow p}/\Gamma_{n\leftrightarrow p}). \tag{32}$$

In Fig. 6 we plot the time evolution of the neutron to proton ratio. In Fig. 6(a) we change only the number of neutrino species in SBBN. The dotted line denote n/p for $N_\nu^{\rm eff}=1.37$ which corresponds to the effective number of neutrino species in the case of $T_R=2$ MeV in the late-time entropy production scenario. Then we find that the predicted n/p curve is lower than that of $N_\nu^{\rm eff}=3$ due to only the speed down effects or the later decoupling. In Fig. 6(b) we plot the time evolution of n/p when we change the reheating temperature in the late-time entropy production scenario. The dotted line denotes the case of $T_R=2$ MeV. Comparing to

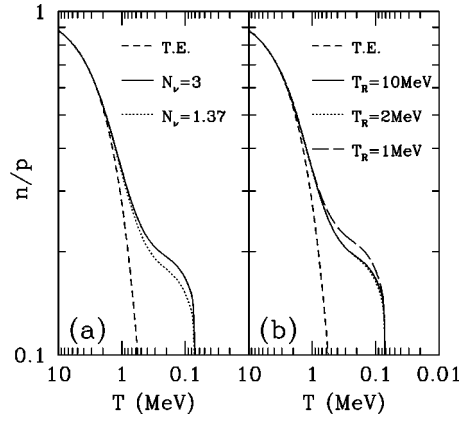

FIG. 6. Evolution of neutron to proton ratio as a function of the temperature, (a) when we change only the number of neutrino species in the standard big bang scenario and (b) when we change the reheating temperature in the late-time entropy production scenario. The dashed line is the thermal equilibrium curve ($=e^{-Q/T}$).

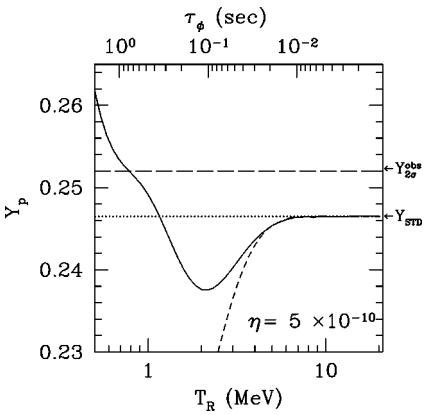

FIG. 7. ^{4}He mass fraction Y_p as a function of T_R (solid line) at $\eta=5\times10^{-10}$. The dashed line denotes the virtual ^{4}He mass fraction computed by including only the speed down effect due to the change of the effective number of neutrino species which is shown in Fig. 4. The dotted line denotes the value predicted in SBBN at $\eta=5\times10^{-10}$. The long-dashed line denotes the observational 2 σ upper bound, $Y^{\rm obs}\sim0.252$ which is obtained by summing the errors in quadrature. The top horizontal axis represents the lifetime which corresponds to T_R.

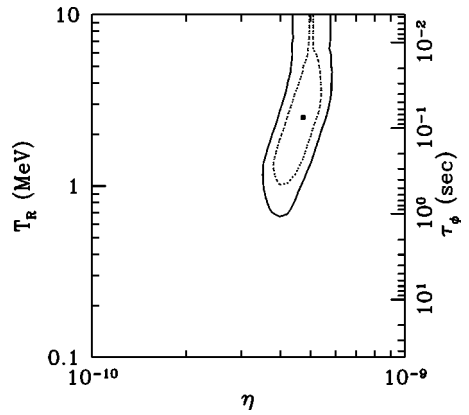

FIG. 8. Contours of the confidence level in (η,T_R) plane. The inner (outer) curve is 68% (95%) C.L. The filled square denotes the best fit point. The right vertical axis denotes the lifetime which corresponds to T_R.

the case of $N_\nu^{\rm eff}=1.37$ in Fig. 6(a), the n/p ratio becomes larger. It is because the weak interaction rates are decreased by the deficit of the distribution function. Moreover in the case of $T_R=1$ MeV the n/p ratio becomes much larger.

C. Neutrino thermalization and light element abundances

Next we perform Monte Carlo simulation and the maximum likelihood analysis [28] to discuss how the theoretical predictions with the low reheating temperature scenario agree with the observational light element abundances. In Fig. 7 we plot the ^{4}He mass fraction Y as a function of T_R at $\eta=5\times10^{-10}$ (solid line). The dashed line denotes the virtual ^{4}He mass fraction computed by including only the speed down effect due to the change of the effective number of neutrino species which is shown in Fig. 4. The dotted line denotes the predicted value of Y in SBBN at $\eta=5\times10^{-10}$. For $T_R\gtrsim7$ MeV, the solid line and dashed line are quite equal to the value in SBBN. As T_R decreases, both the solid and dashed lines gradually decrease because of the speed down effect due to the change of $N_\nu^{\rm eff}$. The dashed line continues to decrease as the reheating temperature decreases.

On the other hand, for $T_R\lesssim2$ MeV the effect that the weak interaction rates are weakened due to the deficit of the neutrino distribution function begins to become important and the predicted value of Y begins to increase as T_R decreases. For $T_R\lesssim1$ MeV, since it is too late to produce enough electrons whose mass is about $m_e=0.511$ MeV, the weak interaction rates are still more weakened and Y steeply increases as T_R decreases.

In Fig. 8 we plot the contours of the confidence level in the η-T_R plane. The solid line denotes 95% C.L. and the dotted line denotes 68% C.L. The filled square is the best fit point between the observation and theoretical predictions. The observational data are consistent with the high baryon to photon ratio $\eta\sim(3-6)\times10^{-10}$. From Fig. 8 we find that $T_R\lesssim0.7$ MeV is excluded at 95 % C.L. In other wards T_R as low as 0.7 MeV is consistent with BBN. Then $N_\nu^{\rm eff}$ can be as small as 0.1 and it definitely influences the formation of the large scale structure and CMB anisotropy as is seen in Sec. VI.

V. HADRON INJECTION BY MASSIVE PARTICLE DECAY

A. Hadron jets and e^+e^- collider experiments

In the previous section we discussed only the case in which the parent massive particle ϕ decays into photons or the other electro-magnetic particles. In this section we consider the entropy production process along with the hadron injection, i.e., the case in which the massive particle has some decay modes into quarks or gluons. Then the emitted quark-antiquark pairs or gluons immediately fragment into hadron jets and as a result a lot of mesons and baryons, e.g., pions, kaons, nucleons (protons and neutrons) are emitted into the electromagnetic thermal bath which is constituted by photons, electrons, and nucleons.

For example, if the gravitino ψ_μ is the parent particle which produces the large entropy, it could have a hadronic decay mode (e.g., $\psi_\mu\to\tilde{\gamma}q\bar{q}$) with the branching ratio $B_h\simeq\mathcal{O}(\alpha)$ at least even if the main decay mode is only $\psi_\mu\to\tilde{\gamma}\gamma$ ($\tilde{\gamma}$: photino) [29]. Then about 0.6–3 hadrons are produced for $m_\phi\simeq1-100$ TeV. In addition the emitted high-energy photons whose energy is about $m_\phi/2$ scatter off the background photons and could also produce the quark-antiquark pairs through the electromagnetic interaction. For the cosmic temperature $\simeq\mathcal{O}$(MeV), the energy in the center of mass frame is $\sqrt{s}\simeq2-20$ GeV for $m_\phi\simeq1-100$ TeV. Then the number of the produced hadrons is about 2–7 which effectively corresponds to the hadron branching ratio $B_h\sim10^{-2}$ if we assume that the hadron fragmentation is similar to the results of e^+e^- collider experiments. Thus B_h should not become less than about 10^{-2} for gravitino

decay.[6] For the other candidate, if the ''flaton'' is the parent particle as in thermal inflation model, it would also have a hadronic decay mode ($\phi \to gg$) [3] if the flaton mass is larger than 1 GeV.

If once such hadrons are emitted to the electromagnetic thermal bath in the beginning of the BBN epoch (at $T \simeq 10$–0.1 MeV), they quickly transfer all the kinetic energy into the thermal bath through the electromagnetic interaction or the strong interaction. Through such thermalization processes the emitted high-energy hadrons scatter off the background particles, and then they induce some effects on BBN. Especially, the emitted hadrons extraordinarily interconvert the ambient protons and neutrons through the strong interaction even after the freeze-out time of the neutron to proton ratio n/p. For the relatively short lifetime ($\tau_\phi \simeq 10^{-2}$–10^2 sec) in which we are interested, the above effect induces the significant change in the previous discussion. Namely, protons which are more abundant than neutrons are changed into neutrons by the hadron-proton collisions and the ratio n/p increases extremely. Because ^{4}He is the most sensitive to the freeze out value of n/p, the late-time hadron injection scenario tends to increase Y_p.

Reno and Seckel [30] investigated the influences of the hadron injection on the early stage of BBN. They constrained the lifetime of the parent particle and the number density comparing the theoretical prediction of the light element abundances with the observational data. Here we basically follow their treatment and apply it to the scenario of late-time entropy production with hadron injections.

The emitted hadrons do not scatter off the background nucleons directly. At first hadrons scatter off the background photons and electrons because they are much more abundant than nucleons. For $t \lesssim 200$ sec, the emitted high-energy hadrons are immediately thermalized through the electromagnetic scattering and they reach kinetic equilibrium before they interact with the ambient protons and neutrons. Then we use the threshold cross section $\langle \sigma v \rangle^{H_i}_{N \to N'}$ for the strong interaction process $N + H_i \to N' + \cdots$ between hadron H_i and the ambient nucleon N, where N denotes proton p or neutron n. The strong interaction rate is estimated by

$$\Gamma^{H_i}_{N \to N'} = n_N \langle \sigma v \rangle^{H_i}_{N \to N'} \simeq 10^8 \ \text{sec}^{-1} f_N \times \left(\frac{\eta}{10^{-9}} \right) \left(\frac{\langle \sigma v \rangle^{H_i}_{N \to N'}}{10 \ \text{mb}} \right) \left(\frac{T}{2 \ \text{MeV}} \right)^3, \quad (33)$$

where n_N is the number density of the nucleon species N, η is the baryon to photon ratio ($= n_B/n_\gamma$), n_B denotes the baryon number density ($= n_p + n_n$), and f_N is the nucleon fraction ($\equiv n_N/n_B$). This equation shows that every hadron whose lifetime is longer than $\mathcal{O}(10^{-8})$ sec contributes to the interconverting interaction between neutron and proton at the beginning of BBN. Hereafter we will consider only the following long-lived hadrons (mesons, $\pi^\pm$, $K^\pm$, and K_L and baryons p, $\bar{p}$, n, and $\bar{n}$). For the relevant process ($N + \pi^\pm \to N' \cdots$ and $N + K^- \to N' \cdots$, etc.), we can obtain the cross sections in Refs. [30,31]. Here we ignore the K^+ interaction because $n + K^+ \to p + K^0$ is the endothermic reaction which has $Q = 2.8$ MeV.

[6] If the decay mode $\psi_\mu \to \tilde{g} g (\tilde{g}$: gluino) is kinematically allowed, the hadronic branching ratio becomes close to 1.

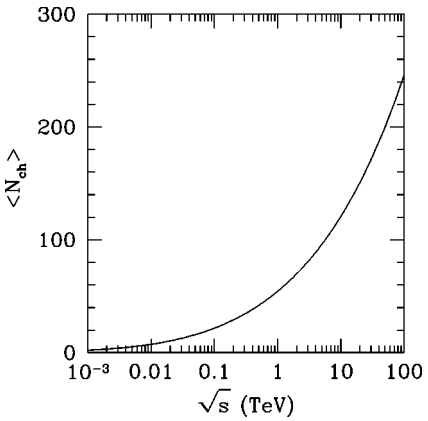

FIG. 9. Plot of the charged particle multiplicity $\langle N_{\rm ch} \rangle$ for the center of mass energy $\sqrt{s} = 1$ GeV $-$ 100 TeV.

We estimate the average number of emitted hadron species H_i per one ϕ decay as

$$N^{H_i} = B_h N_{\rm jet} f_{H_i} \frac{\langle N_{\rm ch} \rangle}{2}, \quad (34)$$

where $\langle N_{\rm ch} \rangle$ is the averaged charged-particle multiplicity which represents the total number of the charged particles emitted per two hadron jets, f_{H_i} is the number fraction of the hadron species H_i to all the emitted charged particles, B_h is the branching ratio of the hadronic decay mode, and $N_{\rm jet}$ is the number of the produced jets per one ϕ decay.

Here it is reasonable to assume that the averaged charged particle multiplicity $\langle N_{\rm ch} \rangle$ is independent of the the source because the physical mechanism which governs the production of hadron jets is quite similar and does not depend on the detail of the origin only if the high-energy quark-antiquark pairs or gluons are emitted. We adopt the data which are obtained by the e^+e^- collider experiments. The CERN e^+e^- collider LEPII experiments (Aleph, Delphi, L3, and OPAL) recently gave us the useful data for $\sqrt{s} = 130$–172 GeV [27]. We adopt the following fitting function for $\sqrt{s} = 1.4$–172 GeV [31]:

$$\langle N_{\rm ch} \rangle = 1.73 + 0.268 \exp(1.42 \sqrt{\ln(s/\Lambda^2)}), \quad (35)$$

where $\sqrt{s}$ denotes the center of mass energy, the functional shape is motivated by the next-to-leading order perturbative QCD calculations, Λ is the cutoff parameter in the perturbative calculations and we take $\Lambda = 1$ GeV. In Fig. 9 we plot the charged particle multiplicity for $\sqrt{s} = 1$ GeV $-$ 100 TeV. The error of the fitting is about 10%. Using the available data [27,31,32], we obtain the emitted hadron fraction $f_{H_i} \equiv n^{H_i}/\langle N_{\rm ch} \rangle$,

$$f_{\pi^+}=0.64, \quad f_{\pi^-}=0.64,$$

$$f_{K^+}=0.076, \quad f_{K^-}=0.076, \quad f_{K_L}=0.054 \tag{36}$$

$$f_p=f_{\bar{p}}=0.035, \quad f_n=f_{\bar{n}}=0.034,$$

where n^{H_i} is the number of the emitted hadron species H_i which is defined as the value after both K_S and Λ^0 had completely finished to decay.[7] As we find easily, almost all the emitted particles are pions which are the lightest mesons. To apply the data of the e^+e^- collider experiments, we take $\sqrt{s}=2E_{\rm jet}$ in $\langle N_{\rm ch}\rangle$ where $E_{\rm jet}$ denotes the energy of one hadron jet because the $\langle N_{\rm ch}\rangle$ is obtained by the result for two hadron jets.

B. Formulation in hadron injection scenario

In this section we formulate the time evolution equations in the late-time hadron injection scenario. As we mentioned in the previous section, the hadron injection at the beginning of BBN enhances the interconverting interactions between neutron and proton equally and the freeze out value of n/p can be extremely increased. Then the time evolution equations for the number density of a nucleon $N(=p,n)$ is represented by

$$\frac{dn_N}{dt}+3H(t)n_N=\left[\frac{dn_N}{dt}\right]_{\rm weak}-\Gamma_\phi n_\phi(K_{N\to N'}-K_{N'\to N}), \tag{37}$$

where $H(t)$ is Hubble expansion rate, $[dn_N/dt]_{\rm weak}$ denotes the contribution from the weak interaction rates which are obtained by integrating the neutrino distribution functions as discussed in Sec. IV, see Eqs. (25)–(30), $n_\phi=\rho_\phi/m_\phi$ is the number density of ϕ, $K_{N\to N'}$ denotes the average number of the transition $N\to N'$ per one ϕ decay.

The average number of the transition $N\to N'$ is expressed by

$$K_{N\to N'}=\sum_{H_i} N^{H_i}R^{H_i}_{N\to N'}, \tag{38}$$

where H_i runs the hadron species which are relevant to the nucleon interconverting reactions, N^{H_i} denotes the average number of the emitted hadron species H_i per one ϕ decay which is given by Eq. (34), and $R^{H_i}_{N\to N'}$ denotes the probability that a hadron species H_i induces the nucleon transition $N\to N'$,

$$R^{H_i}_{N\to N'}=\frac{\Gamma^{H_i}_{N\to N'}}{\Gamma^{H_i}_{\rm dec}+\Gamma^{H_i}_{\rm abs}}, \tag{39}$$

where $\Gamma^{H_i}_{\rm dec}=\tau^{-1}_{H_i}$ is the decay rate of the hadron H_i and $\Gamma^{H_i}_{\rm abs}\equiv\Gamma^{H_i}_{N\to N'}+\Gamma^{H_i}_{N'\to N}+\Gamma^{H_i}_{N\to N}+\Gamma^{H_i}_{N'\to N'}$ is the total absorption rate of H_i.

C. Hadron injection and BBN

In this subsection we compare the theoretical prediction of the light element abundances in the hadron injection scenario to the observational light element abundances. In the computations we assume that the massive particle decays into three bodies ($E_{\rm jet}=m_\phi/3$) and two jets are produced at the parton level ($N_{\rm jet}=2$).[8] In the computing we take the branching ratio of the hadronic decay mode $B_h=\mathcal{O}(10^{-2}-1)$.

As we noted in the previous subsections, it is a remarkable feature that the predicted Y_p tends to increase in the hadron injection scenario because ^{4}He is the most sensitive to the freeze-out value of the neutron to proton ratio. Since protons which are more abundant than neutrons are changed into neutrons through the strong interactions rapidly, the freeze out value of n/p increase extremely if once the net hadrons are emitted. In Fig. 10 we plot the predicted ^{4}He mass fraction Y_p as a function of T_R for (a) $m_\phi=100$ TeV and (b) $m_\phi=10$ GeV. The solid curve denotes the predicted Y_p. Here we take the branching ratio of the hadronic decay mode as $B_h=1$ (right one) and $B_h=0.01$ (left one). The dot-dashed line denotes $B_h=0$. The dashed line denotes the virtual value of Y_p computed by including only the speed down effect due to the change of the effective number of neutrino species. The dotted line denotes the prediction in SBBN.

As we mentioned in the previous section, the speed down effect due to deficit of the electron neutrino distribution function are not important for $T_R\gtrsim 7$ MeV. In addition since it is high enough to keep $n/p\simeq 1$ for the cosmic temperature $T\gtrsim 7$ MeV, the enhancements of the interconverting interaction between n and p due to the hadron emission do not induce any changes on the freeze-out value of n/p. As T_R decreases ($T_R\lesssim 7$ MeV), Y_p also decreases gradually because the speed down effect on the freeze-out value of n/p begins to be important. On the other hand, if a lot of hadrons are emitted when the cosmic temperature is $T\lesssim 6$–7 MeV and the ratio n/p is less than 1, they enhance the interconverting interactions more rapidly. As a result, the ratio n/p attempts to get closer to one again although the cosmic tem-

[7]The summation of f_{H_i} is obviously more than 1 because the experimental fitting of $\langle N_{\rm ch}\rangle$ is defined as a value before K_S and Λ^0 decay [32]. Here we assume that f_{H_i} does not change significantly in the energy range $\sqrt{s}\simeq 10$ GeV–100 TeV. Since we do not have any experimental data for the high-energy region more than about 200 GeV, we extrapolate $\langle N_{\rm ch}\rangle$ to the higher-energy regions and we take f_{H_i} as a constant.

[8]The above choice of the set of model parameters $E_{\rm jet}$ and $N_{\rm jet}$ is not unique in general and is obviously model dependent. However, since $\langle N_{\rm ch}\rangle$ has the logarithmic dependence of $E_{\rm jet}$, we should not be worried about the modification of $E_{\rm jet}$ by just a factor of 2. On the other hand in Eq. (37), the second term on the right-hand side scales as $\propto N_{\rm jet}/m_\phi$. For the modification of $N_{\rm jet}$, therefore, we only translate the obtained results according to the above scaling rule and push the responsibility off onto m_ϕ.

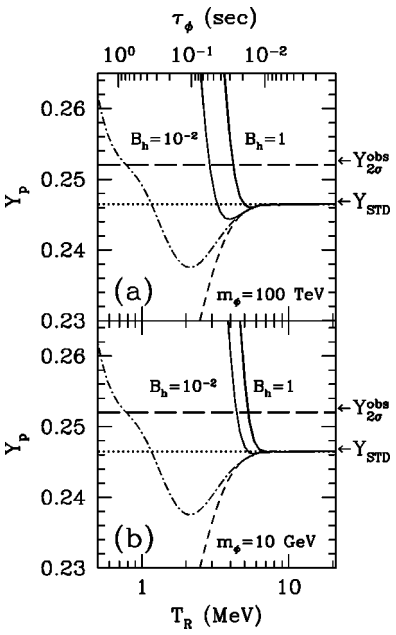

FIG. 10. Plot of the predicted ^{4}He mass fraction Y_p as a function of T_R for (a) $m_\phi=100$ TeV and (b) $m_\phi=10$ GeV at $\eta=5\times10^{-10}$. The solid curve denotes the predicted Y_p where we take the branching ratio of the hadronic decay mode as $B_h=1$ (right one) and $B_h=0.01$ (left one). The dot-dashed line denotes $B_h=0$. The dashed line denotes the virtual Y_p curve computed by including only the speed down effect due to the change of the effective number of neutrino species. The dotted line denotes Y_p in SBBN. The long-dashed line denotes the rough observational two σ upper bound that Y_p should be less than about 0.252. The top horizontal axis represents the lifetime which corresponds to T_R.

perature is still low. Thus the above effects extremely increase the freeze-out value of n/p and is much more effective than the speed down effects. Namely, the produced Y_p becomes larger very sensitively only if T_R is just a little lower than 6–7 MeV. One can obviously find that this effect becomes more remarkable for the larger B_h.

To understand how it depends on mass, it is convenient to introduce the yield variable Y_ϕ which is defined by

$$Y_\phi \equiv n_\phi / s, \tag{40}$$

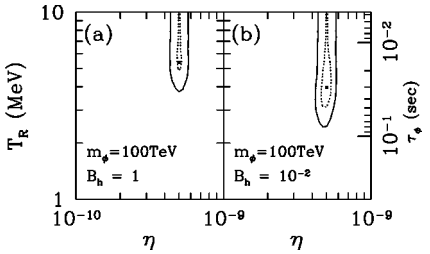

FIG. 11. Contours of the confidence levels for $m_\phi=100$ TeV in (η, T_R) plane for the branching ratio of the hadronic decay mode (a) $B_h=1$ and (b) $B_h=10^{-2}$. The solid line denotes 95% C.L. and the dotted line denotes 68% C.L. The filled square is the best fit point between the observation and theoretical prediction for D, ^{4}He, and ^{7}Li. The right vertical axis represents the lifetime which corresponds to T_R.

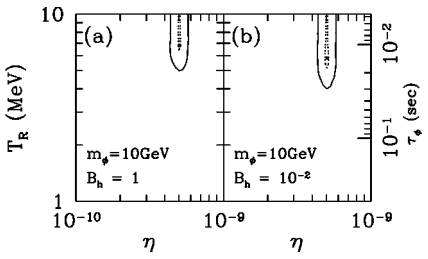

FIG. 12. Contours of the confidence levels for $m_\phi=10$ GeV for the same theory parameters as in Fig. 11.

where s denotes the entropy density in the universe. Because Y_ϕ is a constant only while the universe expands without any entropy production, it represents the net number density of ϕ per comoving volume. For simplicity let us consider the instantaneous decay of ϕ and assume that the reheating process is completed quickly. Because the radiation energy in the thermal bath or entropy $s=2\pi^2 g_*/45 T_R^3$ is produced only from the decay products of ϕ, Y_ϕ is approximately estimated using T_R and m_ϕ by

$$Y_\phi \simeq 0.28 \frac{T_R}{m_\phi}. \tag{41}$$

From the above equation, we can see that for the fixed value of T_R the net number of ϕ, i.e., the net number of the emitted hadrons, becomes larger for the smaller mass. Comparing Fig. 10(a) with Fig. 10(b), we find that the theoretical curve of Y_p for the case of $m_\phi=10$ GeV is enhanced more steeply and the starting point to increase Y_p becomes higher than for the case of $m_\phi=100$ TeV.

Since the other elements (D and ^{7}Li) are not so sensitive as ^{4}He, it is expected that the observational value of Y_p constrains T_R most strongly. In order to discuss how a low reheating temperature is allowed by comparing the theoretical predictions with observational values (D, ^{4}He, and ^{7}Li), we perform the Monte Carlo simulation and maximum likelihood analysis as discussed in Sec. IV. In addition to the case of Sec. IV we take account of the following uncertain-

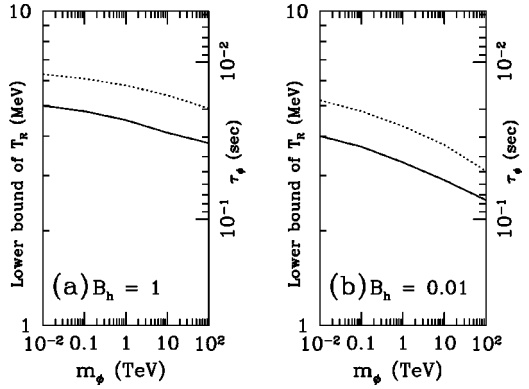

FIG. 13. Lower bound on T_R as a function of m_ϕ for the branching ratio of the hadronic decay mode (a) $B_h=1$ and (b) $B_h=10^{-2}$. The solid line denotes 95% C.L. and the dotted line denotes 68% C.L. The right vertical axis represents the lifetime which corresponds to T_R.

ties, the error for the fitting of $\langle N_{\rm ch}\rangle$ as 10% [31] and the experimental error for each cross section of the hadron interaction as 50%. Because there are not any adequate experimental data for the uncertainties of cross sections [30,31], here we take the larger values to get a conservative constraint.

In Fig. 11 we plot the contours of the confidence level for $m_\phi = 100$ TeV in the (η-T_R) plane for (a) $B_h = 1$ and (b) $B_h = 10^{-2}$. The solid line denotes 95 % C.L., the dotted line denotes 68 % C.L. and the filled square is the best fit point between the observation and theoretical prediction for D, ^{4}He, and ^{7}Li. The baryon to photon ratio which is consistent with the observational data is restricted in the narrow region $\eta \simeq (4-6)\times 10^{-10}$. From Fig. 11(a), we find that $T_R \lesssim 3.7$ MeV is excluded at 95% C.L. for $B_h = 1$. On the other hand, from Fig. 11(b) we obtain the milder constraint that $T_R \lesssim 2.5$ MeV is excluded at 95 % C.L. for $B_h = 10^{-2}$. In Fig. 12 we plot the contours of the confidence level for $m_\phi = 10$ GeV in the same way as Fig. 11. Compared to Fig. 11, as we mentioned above, we find that the lower bound on the reheating temperature becomes higher for a smaller mass. From Fig. 12 we get the lower bound on the reheating temperature that $T_R \gtrsim 5.0$ MeV (4.0 MeV) at 95 % C.L. for $B_h = 1$ ($B_h = 10^{-2}$)

In Fig. 13 the lower bound on T_R as a function of m_ϕ are plotted for (a) $B_h = 1$ and (b) $B_h = 10^{-2}$. The solid line denotes 95 % C.L. and the dotted line denotes 68 % C.L. As is expected, the curve of the lower bound on T_R is a gentle monotonic decreasing function of m_ϕ. In Fig. 13(a), we can see that T_R should be higher than 4 MeV at 95 % C.L. for $B_h = 1$ in $m_\phi = 10$ GeV–10^2 TeV.[9] On the other hand, in Fig. 13(b) we find that the constraint gets milder for $B_h = 10^{-2}$. It is shown that $T_R \lesssim 2.5$ MeV is excluded at 95 % C.L. for $B_h = 10^{-2}$. In Fig. 4 we find that $N_\nu^{\rm eff}$ can be allowed as small as 2.8 for $B_h = 1$ (1.9 for $B_h = 10^{-2}$).

D. Summary of hadron injection

In this section we have seen that the BBN constraint on the reheating temperature becomes much more stringent if a massive particle has a branching to hadrons. For successful BBN the reheating temperature should be higher than 2.5 -4 MeV for the branching ratio $B_h = 1 - 10^{-2}$. The hadron injection generally occurs if the late-time reheating is caused by the heavy particle with mass larger than ~ 1 GeV. Many candidates for the late-time reheating such as SUSY particles and flatons have such large masses and hence the constraint obtained here is crucial in constructing particle physics models based on SUSY or thermal inflation models.

For the lower limit of the reheating temperature, the effective number of the neutrino species $N_\nu^{\rm eff}$ is given by 2.8 and 1.9 for $B_h = 1$ and 10^{-2}, respectively. Since the limiting temperature is close to the neutrino decoupling temperature, the deviation of $N_\nu^{\rm eff}$ from the standard value (i.e., 3) is small and hence the detection may not be easy.

However, from more general point of view, it is possible that light particles with mass $\lesssim 1$ GeV are responsible for the late-time reheating. In this case, as seen in the previous section, the reheating temperatures as low as ~ 0.7 MeV are allowed. For such a low reheating temperature, neutrinos cannot be produced sufficiently. Thus the effective number of the neutrino species $N_\nu^{\rm eff}$ becomes much less than 3. This leads to very interesting effects on the formation of large scale structures and CMB anisotropies, which we discuss in the next section.

VI. CONSTRAINTS FROM LARGE SCALE STRUCTURE AND CMB ANISOTROPY

In this section, we discuss possibility to set constraints on the late-time entropy production from the large scale structure and CMB anisotropies. Hereafter, we only consider flat universe models with cosmological constant which are suggested by recent distant Supernovae (SNe) surveys [33,34] and measurements of CMB anisotropies [35].

The late-time entropy production influences formation of the large scale structure and CMB anisotropies since the matter-radiation equality epoch is shifted if the effective number of neutrino species changes. The ratio of neutrino density to blackbody photon density is $\rho_\nu/\rho_\gamma = (7/8)(4/11)^{4/3} N_\nu$. Therefore the redshift of matter-radiation equality can be written as a function of N_ν:

$$1 + z_{\rm eq} = 4.03\times 10^4 \Omega_0 h^2 \left[1 + \frac{7}{8}\left(\frac{4}{11}\right)^{4/3} N_\nu\right]^{-1}, \quad (42)$$

where Ω_0 is the density parameter and h is the nondimensional Hubble constant normalized by 100 km/s/Mpc.

Let us now discuss distribution of galaxies on large scales. For a quantitative analysis, we define the matter power spectrum in Fourier space as $P(k) \equiv \langle |\delta_k|^2 \rangle$, where δ_k is the Fourier transform of density fluctuations and $\langle\rangle$ denotes the ensemble average. Hereafter, we assume the Harrison-Zel'dovich power spectrum, which is motivated by the inflation scenario, as an initial shape of the power spectrum, i.e., $P(k) \propto k$. As fluctuations evolve in the expanding universe, the shape of the power spectrum is changed. One often introduces the transfer function $T(k)$ to describe this modification of the initial power spectrum as $P(k) = AkT(k)^2$, where A is an arbitrary constant. In case of standard cold dark matter (CDM) dominated models, Bardeen *et al.* [36] found a fitting formula:

$$T(k) = \frac{\ln(1+2.34q)}{2.34q} \times [1 + 3.89q + (16.1q)^2 + (5.46q)^3 + (6.71q)^4]^{-1/4}, \quad (43)$$

where $q = k/\Omega_0 h^2$ Mpc^{-1} when the baryon density is negligible small compared to the total density. It is easy to ex-

[9] Although we have adopted the experimental error of each hadron interaction cross section as 50% in the Monte Carlo simulation because of the lack of data, the lower bound on T_R might become about 10% higher than the above values if we adopt the more severe experimental error of 10% instead of 50%.

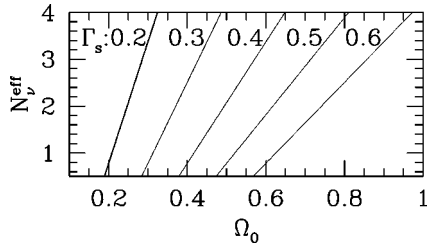

FIG. 14. Contours of $\Gamma_s=0.2$ (bold), 0.3, 0.4, 0.5 and 0.6 on the $(\Omega_0, N_\nu^{\rm eff})$ plane for $h=0.7$.

plain why q is parametrized by $\Omega_0 h^2$. This is because CDM density fluctuations cannot evolve and stagnate during a radiation dominated era. Only after the matter-radiation equality epoch can fluctuations evolve. Therefore the CDM power spectrum has a peak which corresponds to the horizon scale of the matter-radiation equality epoch. In fact, the wave number of the horizon scale at the equality epoch can be written as $k_{\rm eq}=\sqrt{2\Omega_0(1+z_{\rm eq})}H_0$, where H_0 is the Hubble constant at present, that is proportional to $\Omega_0 h^2$. In the actual observations, distances in between galaxies are measured in units of h^{-1} Mpc. Therefore to fit the observational data by the CDM type power spectrum, we usually introduce so-called *shape parameter* $\Gamma_s=\Omega_0 h$. It is known that we can fit the galaxy distribution if $\Gamma_s \simeq 0.25\pm0.05$ [37] which suggests a low density universe. If the late-time entropy production takes place, however, we need to take into account $N_\nu^{\rm eff}$ dependence of the matter-radiation equality epoch [Eq. (42)]. Therefore Γ_s should be written as

$$\Gamma_s = 1.68\Omega_0 h/(1+0.227N_\nu^{\rm eff}). \tag{44}$$

We plot contours of Γ_s on $\Omega_0 - N_\nu^{\rm eff}$ plane in Fig. 14. It is shown that smaller Ω_0 is preferable for $N_\nu^{\rm eff}<3$ with the same value of Γ_s. We also plot the power spectra for $\Omega_0=0.3$ and $h=0.7$ with different $N_\nu^{\rm eff}$'s in Fig. 15. Here we do not simply employ the fitting formula but numerically solve the evolution of density fluctuations [38]. It is shown that the peak location of a model with smaller $N_\nu^{\rm eff}$ shifts to the smaller scale (larger in k) since smaller $N_\nu^{\rm eff}$ makes the equality epoch earlier which means the horizon scale at the equality epoch becomes smaller. We have hope that current large scale structure surveys such as 2DF and Sloan Digital Sky Survey (SDSS) may determine the precise value of Γ_s.

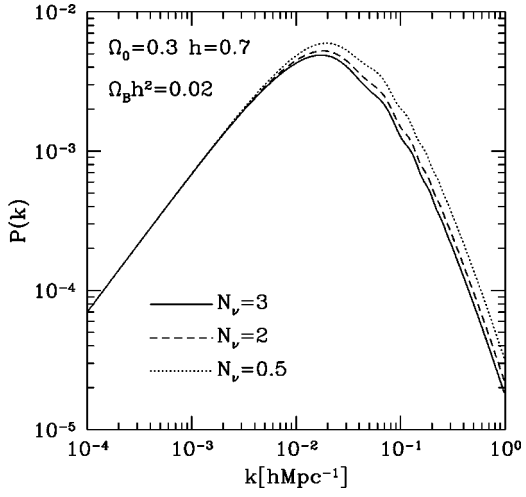

FIG. 15. Matter power spectra $P(k)$ of CDM models with $N_\nu^{\rm eff}=0.5$, 2, and 3. We take $\Omega_0=0.3, h=0.7$, and $\Omega_B h^2=0.02$ where Ω_B is the baryon density parameter.

In addition to the shape of the power spectrum, the amplitude is another important observational quantities to test models. On very large scales, the amplitude of the power spectrum is determined by CMB anisotropies which are measured by COBE/DMR [8]. Since COBE Differential Microwave Radiometer (DMR) scales are much larger than the horizon scale of the matter-radiation equality epoch, however, it is not sensitive to the transfer function $T(k)$ but the overall amplitude A. In order to compare the expected amplitude of the power spectrum from each CDM model with large scale structure observations, we employ the specific mass fluctuations within a sphere of a radius of $8h^{-1}$ Mpc, i.e., σ_8 which is defined as

$$\sigma_8^2 = \langle [\delta M/M(R)]^2 \rangle_{R=8h^{-1}\ {\rm Mpc}} = \frac{1}{2\pi^2}\int dk k^2 P(k) W(kR)^2|_{R=8h^{-1}\ {\rm Mpc}}, \tag{45}$$

where $W(kR)$ is a window function for which we employ a top hat shape as $W(kR)\equiv 3[\sin(kR)-kR\cos(kR)]/(kR)^3$. Eke *et al.* [39] obtained the observational value of σ_8 which is deduced from the rich cluster abundance at present as

$$\sigma_8 = (0.52\pm0.04)\Omega_0^{-0.52+0.13\Omega_0}. \tag{46}$$

Other estimates of σ_8 [40] are agreed with their result. For CDM models with standard thermal history, the value of σ_8 is a function of Ω_0 and h. With the late-time reheating, however, σ_8 for fixed Ω_0 and h becomes larger. The reason is following. Since we fix Ω_0 and h, the normalization factor A is same regardless of the value of $N_\nu^{\rm eff}$. As is shown in Fig. 15, the amplitude of the power spectrum on $8h^{-1}$ Mpc, i.e., σ_8, is larger for smaller $N_\nu^{\rm eff}$. In Fig. 16, we show the allowed region on the $\Omega_0 - h$ plane for $N_\nu^{\rm eff}=0.5$, 2, and 3 for COBE-normalized flat CDM models with the Harrison-Zel'dovich spectrum. The shaded region satisfies the matching condition with the cluster abundance Eq. (46). For fixed h, models with smaller $N_\nu^{\rm eff}$ prefer lower Ω_0. Recently, the HST key project on the extragalactic distance scale has reported that $h=0.71\pm0.06$ (1σ) by using various distant indicators [41]. From SNe measurements, $\Omega_0=0.28\pm0.8$ for flat models (see Fig. 7 of Ref. [34]). CDM models with $N_\nu^{\rm eff}=0.5\sim3$ are still consistent with above value of h and Ω_0. However we expect further precise determination of Ω_0, h (from distant SNe surveys and measurements of CMB anisotropies) and σ_8 (from 2DF or SDSS) will set a stringent constraint on $N_\nu^{\rm eff}$ and T_R in the near future.

Finally we discuss the CMB constraint on T_R. Let us introduce temperature angular power spectrum C_l where l is the multipole number of the spherical harmonic decomposition. The rms temperature anisotropy of CMB can be written

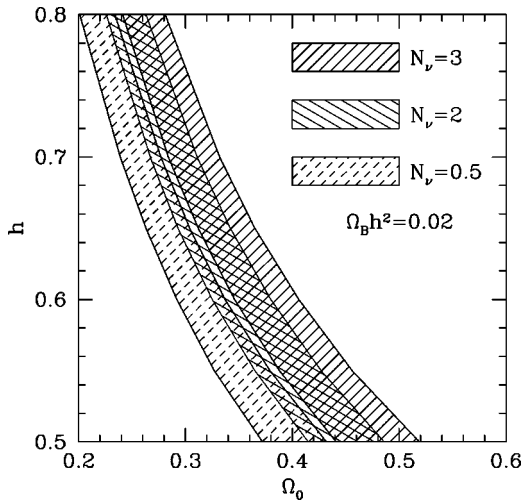

FIG. 16. Allowed region on $\Omega_0 - h$ plane from observational values of σ_8 deduced from the rich cluster abundance at present for flat CDM models. Models with $N_\nu^{\rm eff}=0.5$, 2, and 3 are plotted.

as $\langle|\Delta T/T|^2\rangle = \Sigma_l (2l+1)C_l/4\pi$. Using C_l, we can extract various important information of cosmology, such as the curvature of the universe Ω_0, cosmological constant h, and so on (see, e.g., Ref. [42]). In fact, we can measure the matter radiation equality epoch by using the height of peaks of C_l. The peaks are boosted during the matter-radiation equality epoch. If the matter-radiation equality is earlier, the correspondent horizon scale is smaller. Therefore we expect lower heights for first one or two peaks since these peaks are larger than the horizon scale at the equality epoch and do not suffer the boost as is shown in Fig. 17. With the present angular resolutions and sensitivities of COBE observation [8] or current balloon and ground base experiments, however, it is impossible to set a constraint on $N_\nu^{\rm eff}$. It is expected that future satellite experiments such as MAP [9] and Planck [10] will give us a useful information about $N_\nu^{\rm eff}$. From the Lopez *et al* analysis [7], MAP and Planck have sensitivities that

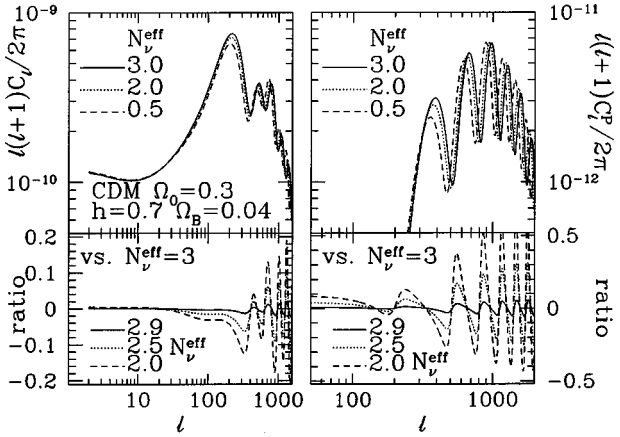

FIG. 17. Power spectra of CMB anisotropies (left top panel) and polarization (right top panel) of models with $N_{\rm eff}^{\rm eff}=3$, 2, and 0.5. Bottom two panels show $[C_l(N_{\rm eff})-C_l(3)]/C_l(3)$ with $N_{\rm eff}^{\rm eff}=2.9$,2.5 and 2 for CMB anisotropies (left bottom) and polarization (right bottom).

$\delta N_\nu^{\rm eff} \gtrsim 0.1$ (MAP) and 0.03 (Planck) including polarization data, even if all cosmological parameters are determined simultaneously (see also Fig. 17). From such future observations of anisotropies of CMB, it is expected that we can precisely determine T_R.

VII. CONCLUSION

In this paper we have investigated the various cosmological effects induced by the late-time entropy production due to the massive particle decay. The neutrino distribution functions have been obtained by solving the Boltzmann equations numerically. We have found that if the large entropy is produced at about $t \simeq 1$ sec, the neutrinos are not thermalized very well and hence do not have the perfect Fermi-Dirac distribution. The deficits of the neutrino distribution functions due to the insufficient thermalization decrease the Hubble expansion rate and weaken the weak interaction rates between proton and neutron. The above two effects change the freeze-out value of n/p significantly. Especially the produced ^{4}He mass fraction Y is so sensitive to n/p that the predicted value of Y is changed drastically. Comparing the theoretical predictions of D, ^{4}He, and ^{7}Li to the observational data, we have estimated the lower bound on the reheating temperature T_R after the entropy production. We have found that $T_R \lesssim 0.7$ MeV is excluded at 95 % C.L. In other wards, T_R can be as low as 0.7 MeV. Then the effective number of neutrino species $N_\nu^{\rm eff}$ can be as small as 0.1. It is enough sensitive for the ongoing large scale structure observations such as 2DF and SDSS or future satellite experiments (MAP and Planck) of CMB anisotropies to detect such modifications on $N_\nu^{\rm eff}$ and we can find out the vestige of the late-time entropy production.

Furthermore, we have also studied the case in which the massive particle has some decay modes into quarks or gluons. In this scenario, a lot of hadrons, e.g., pions, kaons, protons and neutrons, which are originated by the fragmentation of the high-energy quarks and gluons, are injected into thermal bath. The emitted hadrons extraordinarily interconvert the ambient protons and neutrons each other through the strong interaction even after the freeze-out time of the neutron to proton ratio n/p. Then the predicted value of Y increases extremely and we can constrain T_R and the branching ratio of the hadronic decay mode B_h comparing to the observational light element abundances. We have found T_R should be higher than 2.5–4 MeV at 95 % C.L. for $B_h = 10^{-2} - 1$. The above results tell us that $N_\nu^{\rm eff}$ can be as small as 1.9–2.8 even in the hadron injection scenario for $B_h = 10^{-2} - 1$. Then it still may be possible to detect the modifications on $N_\nu^{\rm eff}$ by MAP and PLANCK.

ACKNOWLEDGMENTS

K.K. wishes to thank J. Yokoyama and T. Asaka for useful discussions. This work was partially supported by the Japanese Grant-in-Aid for Scientific Research from the Monbusho, Grant Nos. 10640250 (M.K.), 10-04502 (K.K.), 9440106 (N.S.), and ''Priority Area: Supersymmetry and

Unified Theory of Elementary Particles (No. 707)'' (M.K.) and by the Sumitomo Foundation (N.S.).

APPENDIX: REDUCTION OF COLLISION INTEGRAL

This appendix shows how we can reduce the nine-dimensional integrals in Eq. (6) of the collision term $C_{i,\mathrm{scat}}$ for the scattering process into one dimensional integrals. Notice that, since we treat the massless neutrino, the norm of the neutrino momentum equals to its energy $|\boldsymbol{p}_i|=E_i$. Here we divide the collision term into two parts:

$$C_{i,\mathrm{scat}}=-F+B, \tag{A1}$$

where F represents the forward process and B represents the backward process. They are given by

$$F=\frac{g_e}{2E_1}\int\frac{dp_2^3}{2E_2(2\pi)^3}\int\frac{dp_3^3}{2E_3(2\pi)^3}\int\frac{dp_4^3}{2E_4(2\pi)^3}\times(2\pi)^4\delta^4(p_1+p_2-p_3-p_4)S|M|^2\Lambda_F, \tag{A2}$$

$$B=\frac{g_e}{2E_1}\int\frac{dp_2^3}{2E_2(2\pi)^3}\int\frac{dp_3^3}{2E_3(2\pi)^3}\int\frac{dp_4^3}{2E_4(2\pi)^3}\times(2\pi)^4\delta^4(p_1+p_2-p_3-p_4)S|M|^2\Lambda_B, \tag{A3}$$

where $g_e=2$ and the phase space factors are given by

$$\Lambda_F=f_1(E_1)f_2(E_2)[1-f_3(E_3)][1-f_4(E_4)], \tag{A4}$$

$$\Lambda_B=[1-f_1(E_1)][1-f_2(E_2)]f_1(E_3)f_2(E_4). \tag{A5}$$

The integral over d^3p_4 is immediately done using $\delta^3(\boldsymbol{p}_1+\boldsymbol{p}_2-\boldsymbol{p}_3-\boldsymbol{p}_4)$. From the momentum conservation, $|\boldsymbol{p}_4|$ is given by

$$|\boldsymbol{p}_4|^2=E_4^2=E_2^2+2E_2R\cos\eta+R^2, \tag{A6}$$

where $\boldsymbol{R}\equiv\boldsymbol{p}_1-\boldsymbol{p}_3$, $R=|\boldsymbol{R}|$ and $\cos\eta\equiv\boldsymbol{R}\cdot\boldsymbol{p}_2/(|\boldsymbol{p}_2|R)$.

The remaining delta function $\delta(E_1+E_2-E_3-E_4)$ shows the energy conservation low which is given by

$$E_4^2=E_1^2+E_2^2+E_3^2+2(E_1E_2-E_1E_3-E_2E_3). \tag{A7}$$

We can generally take the momentum axes as

$$\boldsymbol{R}=(0,0,R), \tag{A8}$$

$$\boldsymbol{p}_2=(E_2\sin\eta\sin\phi,E_2\sin\eta\cos\phi,E_2\cos\eta), \tag{A9}$$

$$\boldsymbol{p}_3=(E_3\sin\xi,0,E_3\sin\xi), \tag{A10}$$

where

$$\cos\xi=\frac{E_1^2-E_3^2-R^2}{2E_3R}. \tag{A11}$$

Then $|\cos\xi|\leq 1$ demands

$$|E_1-E_3|\leq R\leq E_1+E_3. \tag{A12}$$

The volume element of $\boldsymbol{p}_2$ is given by $dp_2^3=E_2^2d\cos\eta d\phi$ and from Eqs. (A6) and (A7) the azimuthal angle is obtained by

$$\cos\eta=-\frac{R^2-(E_1-E_3)^2-2E_2(E_1-E_3)}{2E_2R}. \tag{A13}$$

Then $|\cos\eta|\leq 1$ demands

$$|E_1-E_3|\leq R\leq E_1+2E_2-E_3. \tag{A14}$$

From Eqs. (A12) and (A14), we can obtain the allowed region of R,

$$|E_1-E_3|\leq R\leq \mathrm{Inf}[E_1+E_3,E_1+2E_2-E_3]. \tag{A15}$$

Since the volume element of $\boldsymbol{p_3}$ is given by $dp_3^2=2\pi E_3^2dE_3d\cos\theta$ where $\cos\theta=\boldsymbol{p}_1\cdot\boldsymbol{p}_3/(E_3E_1)$, the differential angle element is evaluated by

$$d\cos\theta=-\frac{R}{2E_1E_3}dR. \tag{A16}$$

From Eq. (A15) we can see that the integration can be performed in the four allowed intervals

$$\begin{aligned}-F+B&=\frac{1}{128E_1^2}\int_0^\infty dE_3\int_0^\infty dE_2\int dR\int_0^{2\pi}\frac{d\phi}{2\pi}|M|^2\times(-\Lambda_F+\Lambda_B)\\&=\frac{1}{128E_1^2}\Bigg[\int_0^{E_1}dE_3\int_0^{E_3}dE_2\int_{E_1-E_3}^{E_1+2E_2-E_3}dR+\int_0^{E_1}dE_3\int_{E_3}^{\infty}dE_2\int_{E_1-E_3}^{E_1+E_3}dR\\&\quad+\int_{E_1}^{\infty}dE_3\int_{-E_1+E_3}^{E_3}dE_2\int_{-E_1+E_3}^{E_1+2E_2-E_3}dR+\int_{E_1}^{\infty}dE_3\int_{E_3}^{\infty}dE_2\int_{-E_1+E_3}^{E_1+E_3}dR\Bigg]\int_0^{2\pi}\frac{d\phi}{2\pi}S|M|^2\\&\quad\times(-\Lambda_F+\Lambda_B).\end{aligned} \tag{A17}$$

Even though we only show the case of of ν_e here, we can get the same procedure for ν_μ and ν_τ if C_V and C_A are replaced by $\tilde{C}_V$ and $\tilde{C}_A$. As we also noted in Sec. II, we assume that electrons obey the Boltzmann distribution function $e^{-E/T}$. In addition, since neutrinos are massless, the energy momentum conservation gives $p_1\cdot p_4=p_2\cdot p_3$ in the elastic scattering process. The above assumptions simplify the integrations still more.

For the forward reaction $\nu(p_1)+e^{\pm}(p_2)\rightarrow\nu(p_3)+e^{\pm}(p_4)$, the phase space factor is given by

$$\Lambda_F=f_\nu(E_1)[1-f_\nu(E_3)]\exp\left[-\frac{E_2}{T}\right]. \tag{A18}$$

Then F_1 and F_2 in Eq. (12) are analytically estimated as

$$F_1 \equiv \left[\int_0^{E_3} dE_2 \int_{E_1-E_3}^{E_1+2E_2-E_3} dR + \int_{E_3}^{\infty} dE_2 \int_{E_1-E_3}^{E_1+E_3} dR \right] \int_0^{2\pi} \frac{d\phi}{2\pi} \frac{S|M|^2 e^{-E_2/T}}{256(C_V^2+C_A^2)G_F^2}$$
$$= 2T^4[E_1^2+E_3^2+2T(E_1-E_3)+4T^4] - T^2[E_1^2E_3^2 + 2E_1E_3(E_1+E_3)T + 2(E_1+E_3)^2T^2 + 4(E_1+E_3)T^3+8T^4]e^{-E_3/T}, \quad \text{(A19)}$$

$$F_2 \equiv \left[\int_{-E_1+E_3}^{E_3} dE_2 \int_{-E_1+E_3}^{E_1+2E_2-E_3} dR + \int_{E_3}^{\infty} dE_2 \int_{-E_1+E_3}^{E_1+E_3} dR \right] \int_0^{2\pi} \frac{d\phi}{2\pi} \frac{S|M|^2 e^{-E_2/T}}{256(C_V^2+C_A^2)G_F^2}$$
$$= 2T^4(E_1^2+E_3^2-2T(E_1-E_3)+4T^4)e^{(E_1-E_3)/T} - T^2[E_1^2E_3^2+2E_1E_3(E_1+E_3)T+2(E_1+E_3)^2T^2 + 4(E_1+E_3)T^3+8T^4]e^{-E_3/T}. \quad \text{(A20)}$$

On the other hand, for the backward reaction, $\nu(p_1) + e^{\pm}(p_2) \leftarrow \nu(p_3) + e^{\pm}(p_4)$, the phase space factor is given by

$$\Lambda_B = [1-f_\nu(E_1)]f_\nu(E_3)\exp\left(-\frac{E_1+E_2+E_3}{T}\right). \quad \text{(A21)}$$

Then we can analytically obtain B_1 and B_2 in Eq. (12) as

$$B_1 \equiv \left[\int_0^{E_3} dE_2 \int_{E_1-E_3}^{E_1+2E_2-E_3} dR + \int_{E_3}^{\infty} dE_2 \int_{E_1-E_3}^{E_1+E_3} dR \right] \times \int_0^{2\pi} \frac{d\phi}{2\pi} \frac{S|M|^2 e^{-(E_1+E_2+E_3)/T}}{256(C_V^2+C_A^2)G_F^2},$$
$$= 2T^4[E_1^2+E_3^2+2T(E_1-E_3)+4T^4]e^{-(E_1-E_3)/T} - T^2[E_1^2E_3^2+2E_1E_3(E_1+E_3)T+2(E_1+E_3)^2T^2 + 4(E_1+E_3)T^3+8T^4]e^{-E_1/T}, \quad \text{(A22)}$$

$$B_2 \equiv \left[\int_{-E_1+E_3}^{E_3} dE_2 \int_{-E_1+E_3}^{E_1+2E_2-E_3} dR + \int_{E_3}^{\infty} dE_2 \int_{-E_1+E_3}^{E_1+E_3} dR \right] \times \int_0^{2\pi} \frac{d\phi}{2\pi} \frac{S|M|^2 e^{-(E_1+E_2+E_3)/T}}{256(C_V^2+C_A^2)G_F^2}$$
$$= 2T^4[E_1^2+E_3^2-2T(E_1-E_3)+4T^4] - T^2[E_1^2E_3^2 + 2E_1E_3(E_1+E_3)T+2(E_1+E_3)^2T^2+4(E_1+E_3)T^3 + 8T^4]e^{-E_1/T}. \quad \text{(A23)}$$

[1] For a review, see H. P. Nilles, Phys. Rep. **110**, 1 (1984).
[2] C. D. Coughlan, N. Fischler, E. W. Kolb, S. Rabi, and G. G. Ross, Phys. Lett. **131B**, 59 (1983); T. Banks, D. B. Kaplan, and A. E. Nelson, Phys. Rev. D **49**, 779 (1994); B. de Carlos, J. A. Carlos, F. Quevedo, and E. Roulet, Phys. Lett. B **174**, 447 (1993).
[3] D. H. Lyth and E. D. Stewart, Phys. Rev. D **53**, 1784 (1996).
[4] For a review, see G. F. Giudice and R. Rattazzi, Phys. Rep. **322**, 419 (1999); **322**, 501 (1999).
[5] J. Hashiba, M. Kawasaki, and T. Yanagida, Phys. Rev. Lett. **79**, 4525 (1997); T. Asaka, J. Hashiba, M. Kawasaki, and T. Yanagida, Phys. Rev. D **58**, 083509 (1998); T. Asaka and M. Kawasaki, *ibid.* **60**, 123509 (1999).
[6] M. Kawasaki, K. Kohri, and N. Sugiyama, Phys. Rev. Lett. **82**, 4168 (1999).
[7] R. E. Lopez, S. Dodelson, A. Heckler, and M. S. Turner, Phys. Rev. Lett. **82**, 3952 (1999).
[8] C. L. Bennett *et al.*, Astrophys. J. Lett. **464**, L1 (1996).
[9] NRL http://map.gsfc.nasa.gov/
[10] NRL http://astro.estec.esa.nl/SA-general/Projects/Planck/
[11] J. Bernstein, *Kinetic Theory in the Expanding Universe* (Cambridge University Press, Cambridge, England, 1988).
[12] J. Bernstein, L. Brown, and G. Feinberg, Phys. Rev. D **32**, 3261 (1985).
[13] S. Hannestad and J. Madsen, Phys. Rev. D **52**, 1764 (1995).
[14] A. D. Dolgov, S. H. Hansen, and D. V. Semikoz, Nucl. Phys. **B502**, 3 (1997); **B543**, 269 (1999).
[15] M. Srednicki, R. Watkins, and K. Olive, Nucl. Phys. **B310**, 693 (1988).
[16] M. Kawasaki, G. Steigman, and H-S. Kang, Nucl. Phys. **B403**, 671 (1993); M. Kawasaki, P. Kernan, H-S. Kang, R. J. Scherrer, G. Steigman, and T. P. Walker, *ibid.* **B419**, 105 (1994); M. Kawasaki, K. Kohri, and K. Sato, Phys. Lett. B **430**, 132 (1998).
[17] S. Burles and D. Tytler, Astrophys. J. **507**, 732 (1998).
[18] J. K. Webb *et al.*, Nature (London) **388**, 250 (1997).
[19] D. Tytler, S. Burles, L. Lu, X-M. Fan, and A. Wolfe, Astron. J. **117**, 63 (1999).
[20] D. Kirkman, D. Tytler, S. Burles, D. Lubin, and J. O'Meara, astro-ph/9907128.
[21] P. Molaro, P. Bonifacio, M. Centurion, and G. Vladilo, astro-ph/9908060.
[22] K. A. Olive, G. Steigman, and E. D. Skillman, Astrophys. J. **483**, 788 (1997).
[23] Y. I. Izotov, T. X. Thuan, and V. A. Lipovetsky, Astrophys. J., Suppl. Ser. **108**, 1 (1997); Y. I. Izotov and T. X. Thuan, Astrophys. J. **500**, 188 (1998).
[24] B. D. Fields and K. A. Olive, Astrophys. J. **506**, 177 (1998).
[25] P. Bonifacio and P. Molaro, Mon. Not. R. Astron. Soc. **285**, 847 (1997).

[26] E. W. Kolb and M. S. Turner, *The Early Universe* (Addison-Wesley, New York, 1990).
[27] Particle Data Group, C. Caso *et al.*, Eur. Phys. J. C. **3**, 1 (1998).
[28] E. Holtmann, M. Kawasaki, K. Kohri, and T. Moroi, Phys. Rev. D **60**, 023 506 (1999).
[29] S. Dimopoulos, G. Dvali, R. Rattazzi, and G. F. Giudice, Nucl. Phys. **B510**, 12 (1998).
[30] M. H. Reno and D. Seckel, Phys. Rev. D **37**, 3441 (1988).
[31] K. Kohri and J. Yokoyama, Phys. Rev. D **61**, 023501 (2000).
[32] O. Biebel (private communication).
[33] A. G. Riess *et al.*, Astron. J. **116**, 1009 (1998).
[34] S. Perlmutter *et al.*, Astrophys. J. **517**, 565 (1999).
[35] S. Hancock, G. Rocha, A. N. Lasenby, and C. M. Gutiérrez, Mon. Not. R. Astron. Soc. **294**, L1 (1998); G. Efstathiou *et al.*, *ibid.* **393**, L47 (1999); M. Tegmark, Astrophys. J. Lett. **514**, L69 (1999).
[36] J. M. Bardeen, J. R. Bond, N. Kaiser, and A. S. Szalay, Astrophys. J. **304**, 15 (1986).
[37] J. A. Peacock and S. J. Dodds, Mon. Not. R. Astron. Soc. **267**, 1020 (1994).
[38] N. Sugiyama and N. Gouda, Prog. Theor. Phys. **88**, 803 (1992).
[39] V. R. Eke, S. Cole, and C. S. Frenk, Mon. Not. R. Astron. Soc. **282**, 263 (1996).
[40] N. A. Bahcall and X. Fan, Astrophys. J. **504**, 1 (1998); P. T. P. Viana and A. R. Liddle, in *Proceedings of the Conference ''Cosmological Constraints from X-Ray Clusters''* astro-ph/9902245.
[41] J. R. Mould *et al.*, astro-ph/9909260.
[42] W. Hu, N. Sugiyama, and J. Silk, Nature (London) **386**, 37 (1997).